第 43 卷 第 8 期/2023 年 4 月/光学学报 内封底文章·特邀论文

光学学报

基于共聚焦亚像素扫描的高分辨三维成像

黄远建[1,2]，李晓银[1,2]，叶文怡[1,2]，郭迎辉[1,2]，杨龙飞[3]，贺江[3]，柯源[3]，蒲明博[1,2]，罗先刚[1,2*]

[1]中国科学院光电技术研究所微细加工光学技术国家重点实验室，四川 成都 610209；

[2]中国科学院大学电子电气与通信工程学院，北京 101408；

[3]天府兴隆湖实验室，四川 成都 610299

摘要 激光雷达技术因具有高精度、高分辨率和工作距离远等优点被广泛应用于三维成像。然而，受光学系统衍射极限的限制，激光雷达的空间分辨率随着目标距离的增大而显著降低。为解决上述问题，结合共聚焦照明技术和亚像素扫描技术，提出一种聚焦照明亚像素扫描光子计数激光雷达，并在实验室内进行了 10 m 成像实验。结果表明，相较于准直照明光束，采用共聚焦照明光束可将系统空间分辨率由 5.0 mm 提高到 0.9 mm，不仅实现了超光学系统衍射极限成像，还有效降低了多重回波的影响，增强了回波强度。

关键词 光学设计；激光雷达；亚像素扫描；共聚焦照明；高分辨率

中图分类号 TN958.98 **文献标志码** A **DOI**：10.3788/AOS221974

1 引 言

激光雷达(LiDAR)是一种以脉冲激光或连续激光为光源的主动光学三维成像技术，其工作原理是向被测目标发射激光束，然后测量反射或散射信号的到达时间、强弱程度等参数，以确定目标的距离、方位、运动状态及表面光学特性，从而建立测量目标的三维成像信息。目前激光雷达在地形测绘[1-2]、城市建模[3-4]、工业制造[5-6]、自动驾驶[7-8]等领域已得到广泛的应用，具有良好的应用前景。

随着激光雷达应用范围的不断扩展，对激光雷达成像的要求越来越高，远距离高精度激光三维成像成为国内外学者研究的重点。2005 年麻省理工学院林肯实验室成功研制了 Jigsaw 单光子激光雷达[9]，利用 32×32 盖革模式雪崩光电二极管阵列实现了 150 m 处 40 cm 分辨率，成功恢复出隐藏在伪装网和树叶下的车辆。2013 年，中国科学院上海技术物理研究所研制的多元扫描单光子激光雷达成功辅助“嫦娥 3 号”实现月球软着陆[10]，实现了低于 0.2 m 的探测精度。2014 年，Kirmani 等[11]在每个像素点仅接收一个光子的情况下，利用现实场景中的空间相关性和低通量测量的物理特性，实现了人体模型高分辨三维重建。2017 年，Buller 小组利用铟镓砷单光子探测器(SPAD)，结合全变差优化算法，成功恢复出 10.5 km 处 38°斜坡[12]。2021 年，Li 等[13]利用搭建的 1550 nm 光子计数激光雷达系统，通过匹配探测器接收视场角(FoV)和出射光束发散角，采用时间选通等高效抑噪手段，实现了 201.5 km 处山峰精确成像。然而受限于光学衍射极限，当成像距离拓展至 km 级，空间分辨率严重降低。目前，尽管已报道的单光子激光雷达[14-16]在成像距离方面取得了很大突破，但是他们大多使用准直高斯光束，当成像距离达到 km 甚至数百 km 量级时，由于存在激光发散角，空间分辨率会急剧下降。

减小目标处激光光斑尺寸是一种提高成像分辨率的有效方法，已经被广泛应用在显微成像等领域，例如：2012 年霍华德·休斯医学院的 Gao 等[17]利用贝塞尔光束实现了对活体样品超衍射极限的快速三维成像；2017 年，特拉维夫大学的 Singh 等[18]利用超振荡光束在高分辨捕获方面实现了远超标准衍射极限光束的定位精度；2019 年，南洋理工大学的 Perinchery 等[19]利用贝塞尔光束显微系统对 0.2 μm 荧光球成功成像，实现了亚瑞利分辨率成像。上述研究工作的核心思想都是减小光斑的尺寸，然而该方法在望远成像领域还鲜有应用。此外，亚像素扫描提供了一种相对简单的方法来提高单光子激光雷达的分辨率。通过将扫描步长控制在单个像素尺度内，捕获一系列低分辨率图像，通过计算将多幅低分辨率图像组合生成更高分辨率的图像，如：2020 年，Li 等[20]设计了基于亚像素扫描的单光

收稿日期：2022-11-14；**修回日期**：2022-12-26；录用日期：2022-12-30；**网络首发日期**：2023-02-07

基金项目：国家自然科学基金(61875253，62222513，61975210)、四川省重点研发计划(2021ZYCD001、2020YFJ0001)、中国科学院青年创新促进会(20190731)

通信作者：*lxg@ioe.ac.cn

子激光雷达，实现了 8.2 km 处 5 cm 分辨率；2021 年，Xue 等[21]利用亚像素扫描方法将 3 m 处空间分辨率由 3 mm 提高到 0.33 mm；2021 年，郭静箐等[22]利用亚像素扫描和自适应噪声阈值的多距离重建算法实现了 3.1 km 外目标成像，空间分辨率为 0.11 m。

针对激光雷达成像分辨率受限的问题，结合小光斑照明和亚像素扫描的优势，本文设计了一种工作在 1550 nm 的可变焦光子计数激光雷达，在室内进行验证实验，通过聚焦照明有效降低了多重回波，实现了 10 m 处 0.9 mm 狭缝成像，其空间分辨率超过光学系统的衍射极限。

2　方案设计

2.1　激光扫描三维成像

激光扫描三维成像中，光束通过逐点扫描的方式对目标进行扫描照明，并探测目标不同位置的返回光信号，获取探测目标表面的深度信息，从而实现三维成像。在该过程中，照明光斑在成像目标上的尺寸与分布是成像分辨率的一个重要影响因素，光斑尺寸越小，获得的目标表面信息越精细，重建恢复的物体三维信息越清晰。传统激光扫描三维成像为了减小光束的发散角，一般将激光准直扩束后以平行光束的模式照射至远处目标物体，目标物体处的光斑尺寸主要取决于扩束后的光束发散角以及成像工作距离，且通常情况下远大于衍射极限下的光斑尺寸。光斑尺寸的增大对激光扫描三维成像质量的影响主要体现在两方面：一方面会使照射到物体表面的光信号能量降低，导致返回光信号变弱，从而影响探测距离；另一方面，大光斑照射到物体表面的面积也较大，从而导致同一光斑因为物体面形的变化产生多回波信号，影响测距的精度。为了实现远距离高分辨三维成像，针对上述问题，提出一种基于共聚焦扫描的三维成像方法，其结构示意图如图 1 所示。将平行照明光束改为聚焦照明光束，借助共聚焦扫描的特点，对接收视场与发射视场进行匹配，在保证高扫描精度的同时降低回波噪声。

成像系统的分辨率受限于光学衍射极限，该极限主要取决于光学系统的口径。对于平行照明光束，为了减小光束发散角，需要增大光束的束腰半径，因此需要采用大口径的光学系统进行光束收发。平行照明光斑的大小主要取决于发射光斑直径（D）、光束发散角（θ）和工作距离（L），目标处光斑尺寸的计算公式为

$$D_{\text{target 1}} \approx D + L \times \tan\theta \approx D + L \times \theta。\tag{1}$$

假设在 10 km 的远距离成像场景，发射光斑直径 $D=300$ mm，光束发散角 $\theta=35$ μrad，由式（1）可计算得到目标处光斑直径 $D_{\text{target 1}} \approx 650$ mm。对于聚焦照明，聚焦光斑可通过衍射极限公式近似得到：

$$D_{\text{target 2}} \approx \frac{2.44\lambda}{D} \times L。\tag{2}$$

从式（2）可以看到，聚焦照明光斑大小主要取决于发射光斑直径（D）、激光波长（λ）和工作距离（L）。如图 1（b）所示，根据光焦度（$\Phi=1/f$，焦距的倒数）的计算公式 $\Phi=\Phi_1+\Phi_2-d\Phi_1\Phi_2$，通过改变透镜之间的距离 d，将光斑以聚焦的形式照射至物体表面，在焦深范围内，可实现近衍射极限尺度的照明。在相同的准直照明场景下，将 $L=10$ km、$D=300$ mm、$\lambda=1550$ nm 代入式（2）可得 $D_{\text{target 2}} \approx 126$ mm。在目标处，准直光束照明时光斑大小约为聚焦光束照明光斑大小的 5.1 倍。

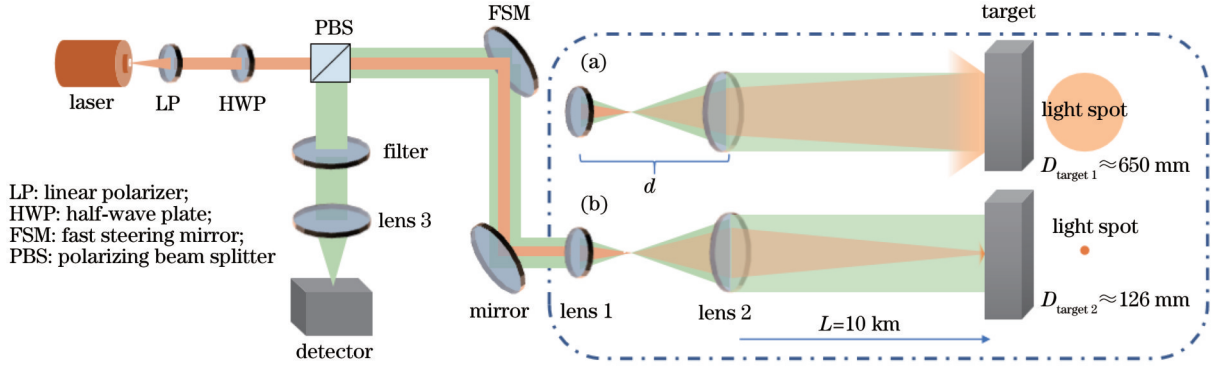

图 1　不同照明方式下激光三维成像原理图。（a）准直照明；（b）聚焦照明

Fig. 1　Schematic of laser 3D imaging under different illumination modes. (a) Collimated illumination; (b) focused illumination

2.2　亚像素扫描超分辨方法

亚像素扫描最初是针对普通数码相机提出的一种从多幅低分辨率（LR）图像获取高分辨率（HR）图像的方法[23]，已被广泛应用在医学成像[24]、卫星成像[25]和视频制作[26-27]等领域。在亚像素扫描技术中，提高空间分辨率的前提是对同一场景以小于最小像素间距的精细步长来获得多幅 LR 图像，通过像素间的重叠采样来获得更多的图像细节信息。如果 LR 图像以像素间距整数单位移位，则每幅图像都包含相同的信息，因此不存在可用于重建 HR 图像的新信息。

类比到激光雷达，同样可以采用亚像素扫描方法来增强系统成像分辨性能。对于激光雷达，单点探测

的FoV等同于一个像素点尺寸，为了平衡探测效率和环境背景噪声的矛盾，通常设置系统接收视场角稍小于激光发散角，此时逐像素扫描中扫描步长等于FoV，而亚像素扫描中的扫描步长小于FoV。在获得多幅LR图像后，亚像素扫描超分辨技术至关重要的一点便是对多幅LR图像重叠的部分提取出更多的细节信息。图2中，对于一个由3×3方格单元组成的图像，系统模拟探测FoV覆盖2×2个方格单元，系统扫描步长为1个方格单元（即以FoV的一半为步长进行亚像素扫描），方格下方标注的数字表示亚像素扫描的顺序。对1中（1 2 4 5）位置进行1/2亚像素扫描，目标像素由2×2（LR）变为4×4（HR）。对于单点激光雷达，只需简单地按照扫描过程排序即可。

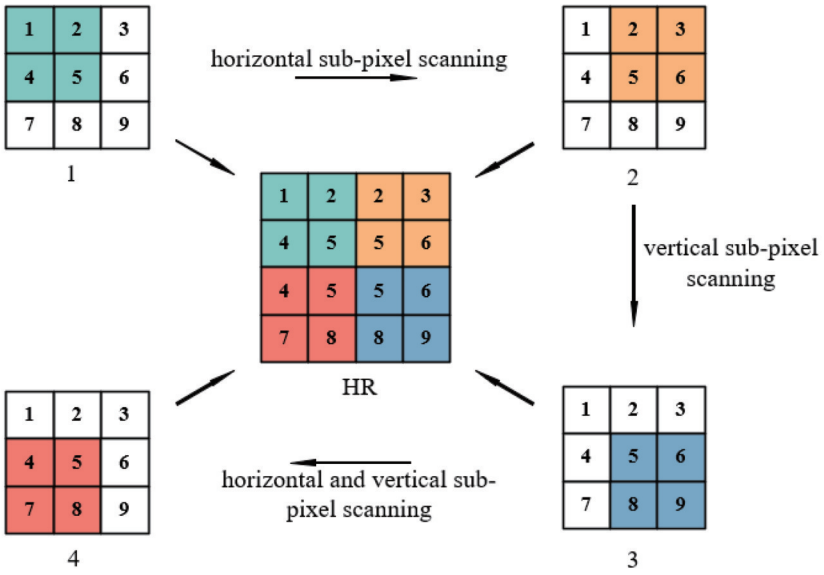

图2　亚像素扫描时的像素点排布示意图

Fig. 2　Schematic of pixel points layout under sub-pixel scanning

3　实验装置

实验装置如图3所示，采用共轴设计和时间相关光子计数（TCSPC）技术。TCSPC技术针对离散光子信号，通过将不同飞行时间划分到离散的时间栅格，对响应以直方图的形式进行积分，能有效减少随机误差，获得精确的时间信息。系统使用出射激光波长为1550 nm的光纤激光器，该激光器以12.7 MHz的重复频率产生脉宽为2.315 ps的脉冲激光。1550 nm工作波段具有对人眼安全、低太阳背景噪声和低大气损耗的优点，有利于后期开展场外实验。激光器通过准直器出射直径为2.0 mm的光束，发散角为1.0 mrad，该光束通过10倍扩束后以水平偏振方向通过偏振分束镜，再经过快反镜和2倍望远镜投射到目标，通过调节望远镜物镜和目镜之间的距离切换准直和聚焦照明模式。准直出射时，光束不经过10倍扩束，因此通过望远镜后，发散角变为0.5 mrad。

共聚焦激光雷达系统的参数如表1所示。探测器接收端采用直径D=50 μm的多模光纤，相比于单模光纤，多模光纤在限制接收视场角的同时能有效提高对回波光子的耦合。耦合透镜焦距f=100 mm，准直和聚焦出射光束时等效焦距f≈200 mm，因此系统接收视场角为$2\times\arctan(D/2f)$=250 μrad。从图3可以看出，激光器和SPAD都是通过光纤跳线连接至发射和接收光路中。因此，在实验过程中可灵活地更换不同直径的光纤、激光器和SPAD，以便满足不同的实验需求。其中快反镜（Newport，FSM300）的扫描重复精度小于3 μrad，保证了亚像素扫描能力，其驱动信号由PLC（Simatic，S7-1200）提供，通过LabVIEW编写的上位机软件对其进行控制。在1 m处放置漫反射片（Thorlabs，DG10-1500-P01），测得系统时间抖动为48 ps，等效测距精度为7.2 mm，分辨率可达到亚厘米级。时间抖动主要包括探测器响应时间抖动、激光源抖动和激光脉宽、计时电路抖动和其他仪器设备的抖动。

由于自然成像目标表面粗糙，所有反射都近似于漫反射，能够显著改变回波光的偏振态。当表面粗糙

表1　共聚焦激光雷达系统参数

Table 1　Parameters of confocal lidar system

Parameter	Value
Wavelength /nm	1550
Laser pulse width /ps	2.315
Laser repetition rate /MHz	12.7
FoV of the detector /μrad	250
Collection fiber /μm	50
Scanning resolution /μrad	3
System time jitter /ps	48

度足够大时，回波光将从水平偏振完全退化为随机偏振，理想情况下，一半回波光的偏振方向与出射光方向正交。尽管至少损失了一半的能量，但在过滤掉后向反射等噪声后，信噪比显著提升。

为了有效验证系统的成像性能，分别对分辨率靶[图 3(b)]和立体玩偶[图 3(c)]进行成像实验。图 3(b)是自行设计、3D 打印的分辨率靶，尺寸为 7.3 cm×7.3 cm，其中所有缝的高度均为 10.0 mm，第一行从左至右的缝宽和缝间距依次为 0.9 mm、3.0 mm 和 5.0 mm，中间行“I”“E”的线条宽度为 2.0 mm，第三行缝宽为 5.0 mm。图 3(c)所示的熊猫玩偶的尺寸为 45.0 mm×43.5 mm×52.0 mm，斜向摆放时脚和鼻子的深度差为 18.0 mm。分辨率靶主要用于评估准直照明和聚焦照明探测图像以及亚像素扫描图像的横向分辨率，熊猫玩偶主要用于观测深度信息对横向分辨率提升的影响。

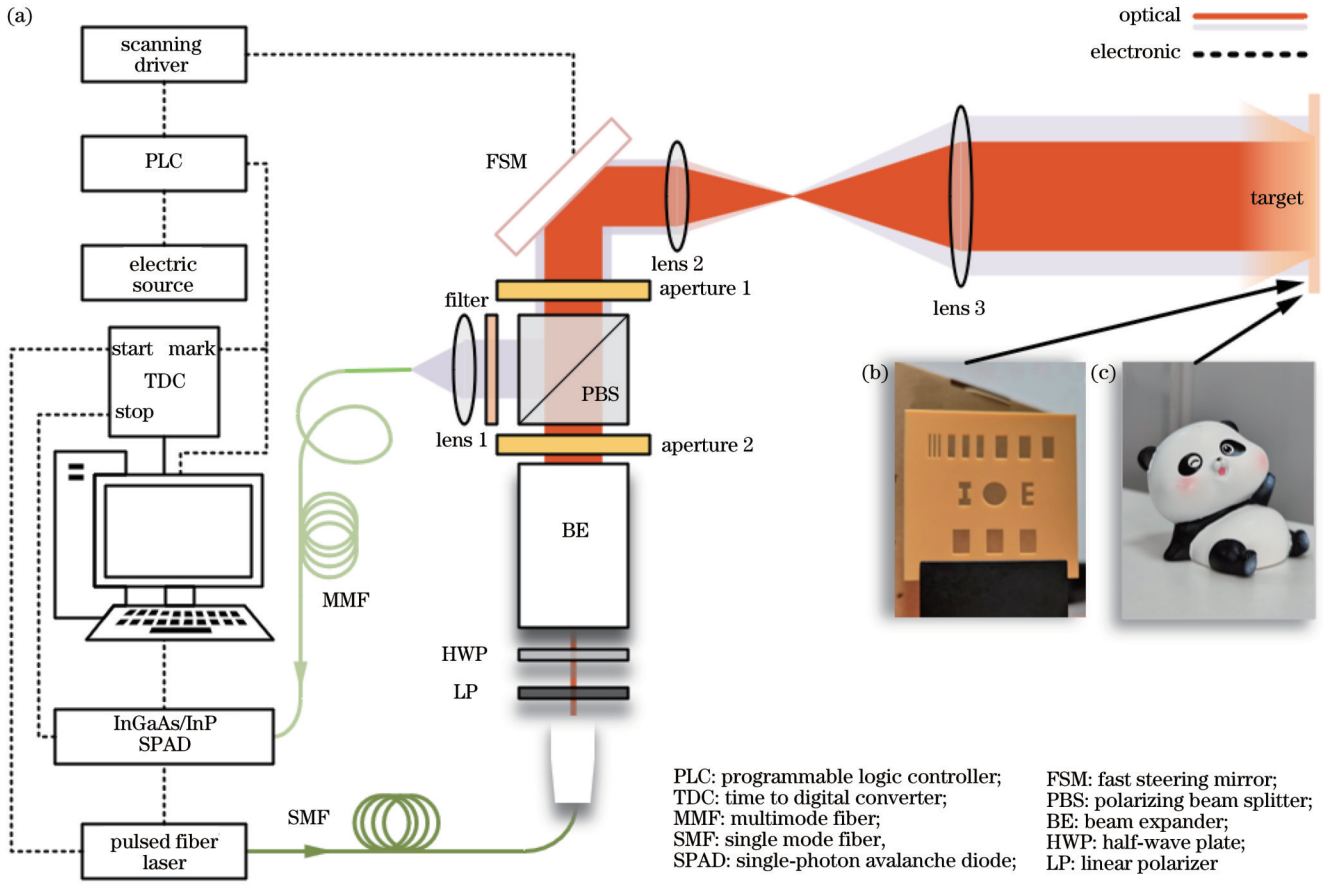

图 3　共聚焦亚像素扫描装置设计。(a)装置原理图；(b)分辨率靶；(c)熊猫玩偶

Fig. 3　Design of confocal sub-pixel scanning device. (a) Device schematic; (b) resolution target; (c) panda doll

4　实验结果和分析

4.1　分辨率靶

为了定量表征系统的横向和纵向分辨率，将自制的透射式分辨率靶依次放置在距离发射端 7、8、10 m 处，并在其后 15 cm 处斜向 33.3°放置一个纸箱子。分别用准直光束和聚焦光束以 250 μrad(逐像素)、62.50 μrad(1/4 亚像素)、31.25 μrad(1/8 亚像素)步长进行扫描。准直光束照明时，7、8、10 m 处光斑直径分别为 8.0、8.6、9.5 mm；聚焦照明时，7、8、10 m 处光斑直径分别为 1.6、1.8、2.3 mm。250 μrad 和 62.50 μrad 步长扫描时单点凝视时间为 10 ms，31.25 μrad 步长扫描时单点凝视时间为 5 ms。在 12.7 MHz 的同步信号下，SPAD 工作在固定门控状态，门控开启时间为 6 ns，设定 10 ns 延迟，以滤掉后向反射噪声和 PBS 处泄漏的能量。对于深度估计，使用一种简单的计算方法：先对测得的系统仪器响应函数曲线用二分段高斯函数进行拟合，再用测得的参数对每个像素位置的光子直方图进行拟合，通过搜索最大值法获得拟合曲线中的峰值位置和强度信息。

图 4 展示了于 7 m 和 10 m 处利用准直光束照射分辨靶时得到的深度图。对于准直照明，无论是否使用亚像素扫描方法，在 7 m 和 10 m 处都只能得到大致轮廓，无法准确恢复分辨率靶的形貌。对比 250 μrad 步长扫描，在 7 m 处能恢复“I”部分轮廓，而在 10 m 处只能识别“I”位置存在孔洞，符合距离越远，接收面越大，成像分辨率越低的一般规律。为了解亚像素扫描对成像质量的改善效果，评估了目标相同部分平面区域的横向精度。图 4 第一列是在 7 m 处以 250 μrad 和 31.25 μrad 扫描得到的深度信息的局部放大图，可以看

到，相比于250 μrad的逐像素步长步长扫描，31.25 μrad的1/8亚像素扫描能够恢复字母“I”的上下两端。此外，亚像素扫描重建图像相比于逐像素扫描图像更为平滑，细节恢复得更好，字母“E”从完全无法分辨到能初窥形貌。因此，对于准直照明，亚像素扫描对成像分辨率的提升效果有限，无法识别0.9 mm狭缝。

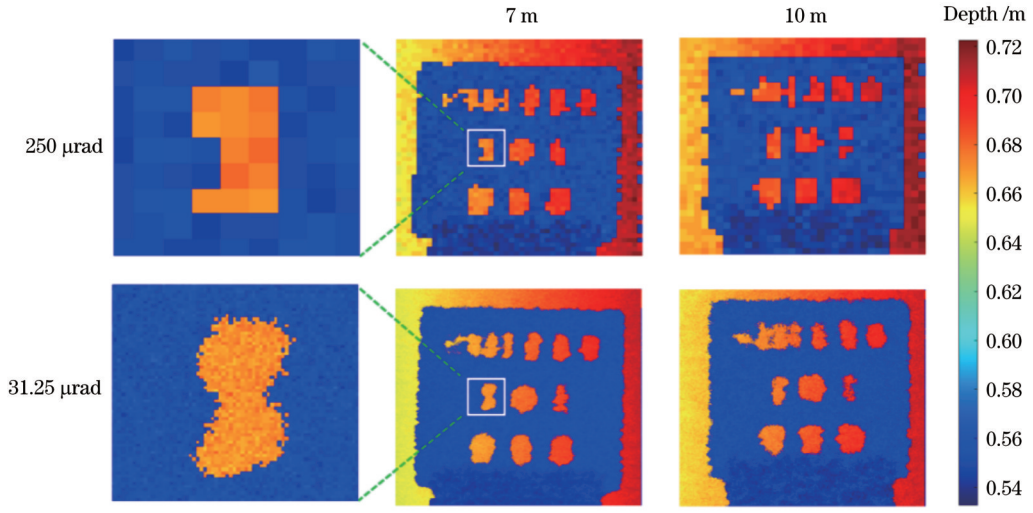

图4　准直光束照明时分辨率靶深度图

Fig. 4　Resolution target depth maps under collimated beam illumination

从图4还可以看到，受到激光多重回波反射的影响，透射式分辨率靶的边缘出现很多毛刺。具体地说，在接收视场内，部分光透过狭缝照射在纸箱，部分光照亮分辨率靶，存在不同深度信息，因此出现两个峰。而两个峰的强度随着扫描位置的变化而变化，从而导致无法准确获得该位置的深度信息。图5所示为8 m处准直光束照射在某一条缝边缘时的回波信号，第一个峰的横坐标对应分辨率靶的位置，第二个峰是穿过狭缝照射背后纸箱时返回的信号。当光束小幅度移动，回波信号便从图5(a)的第一个峰强变成图5(b)的第二个峰强，因此无法判断该点是属于分辨率靶还是属于背后纸箱。图5(c)所示为在相同接收视场角和出射功率下测量8 m处的漫反射率靶，累计5 s后得到的光子直方图，其中虚线代表聚焦照明，实线表示准直照明，聚焦照明的峰值强度约为准直照明峰值强度的3.4倍。可见，聚焦照明不但能提升系统分辨率，还能明显增加系统的探测能量。

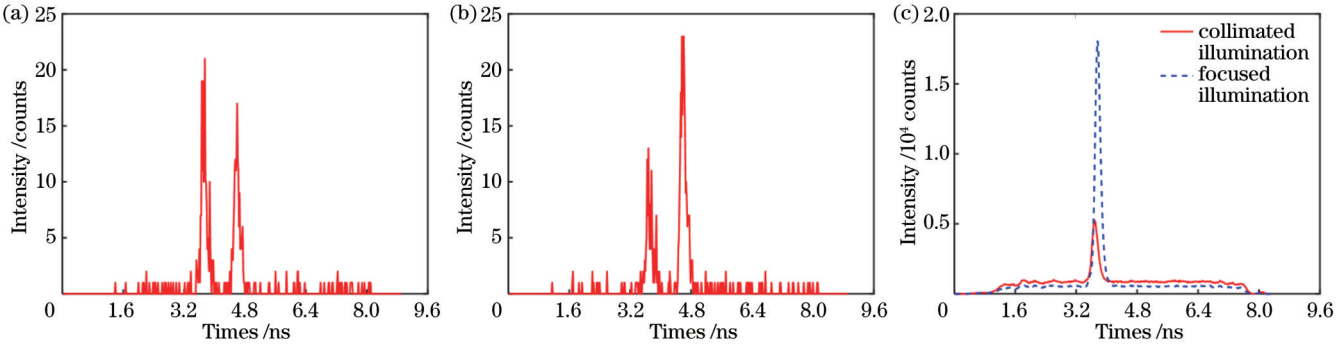

图5　不同位置的回波强度直方图及强度对比结果。(a)初始位置的强度直方图；(b)小位移偏移后的强度直方图；(c)准直照明和聚焦照明强度对比

Fig. 5　Echo intensity histograms at different positions and comparison result of intensity. (a) Histogram at initial position; (b) histogram after small displacement offset; (c) intensity comparison of collimated illumination and focused illumination

图6给出了8 m处准直照明和聚焦照明以逐像素和1/8亚像素步长扫描的深度图像成像结果，中间两列为“E”的局部放大图。同样是逐像素扫描，聚焦照明能够准确恢复“E”的形貌，且其余狭缝相比于准直照明缺失和凸起部分大大减少，说明小光斑照明能有效降低多重回波的影响。此外，1/8亚像素扫描时，聚焦照明成功恢复出所有孔洞，0.9 mm缝也清晰可见，而准直照明仍然只能看出大致轮廓，说明在系统本身有一定分辨能力的情况下，亚像素扫描仅能使成像结果更为准确和平滑，并不能显著提升成像分辨率。对于多重回波，已有科研人员研究如何用算法进行处理，如：Yin等[28]在2014年提出一种自适应模拟退火马尔科夫链蒙特卡罗分析方法；Shin等[29]在2016年将多重回波问题转换成稀疏解卷积问题，并通过凸优化求解。可见，使用小光斑进行照明，从源头上抑制多重回波的产生也尤为重要。

标准成像系统的分辨率受到衍射极限的限制，而衍

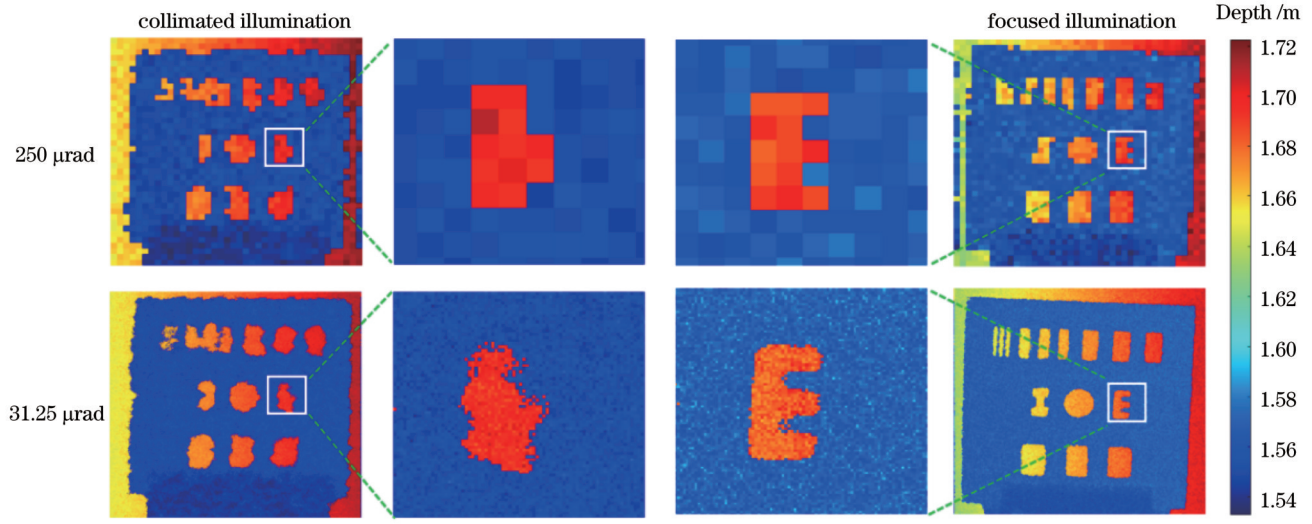

图 6　8 m 处准直光束和聚焦光束照明深度图

Fig. 6　Illumination depth diagrams of collimated beam and focused beam at 8 m

射极限主要由光学系统的孔径决定。通常将单个检测像素的视场 FoV 设为与该衍射极限(艾里斑直径)匹配。在这种情况下，激光雷达系统的角度分辨率 $\Delta\theta=2.44\lambda/D$[20]。以本实验装置为例，激光器波长 $\lambda=1550$ nm，光阑限制后口径 $D=24$ mm，系统极限分辨率约为 158 μrad，8 m 处的分辨率约为 1.3 mm，大于 0.9 mm。可见，通过聚焦光束照明和亚像素扫描可以突破系统极限空间分辨率的限制，实现超衍射极限成像。

不同程度的亚像素扫描对成像分辨率的影响如图 7 所示，其中第一行是 0.9 mm 缝成像结果的局部放

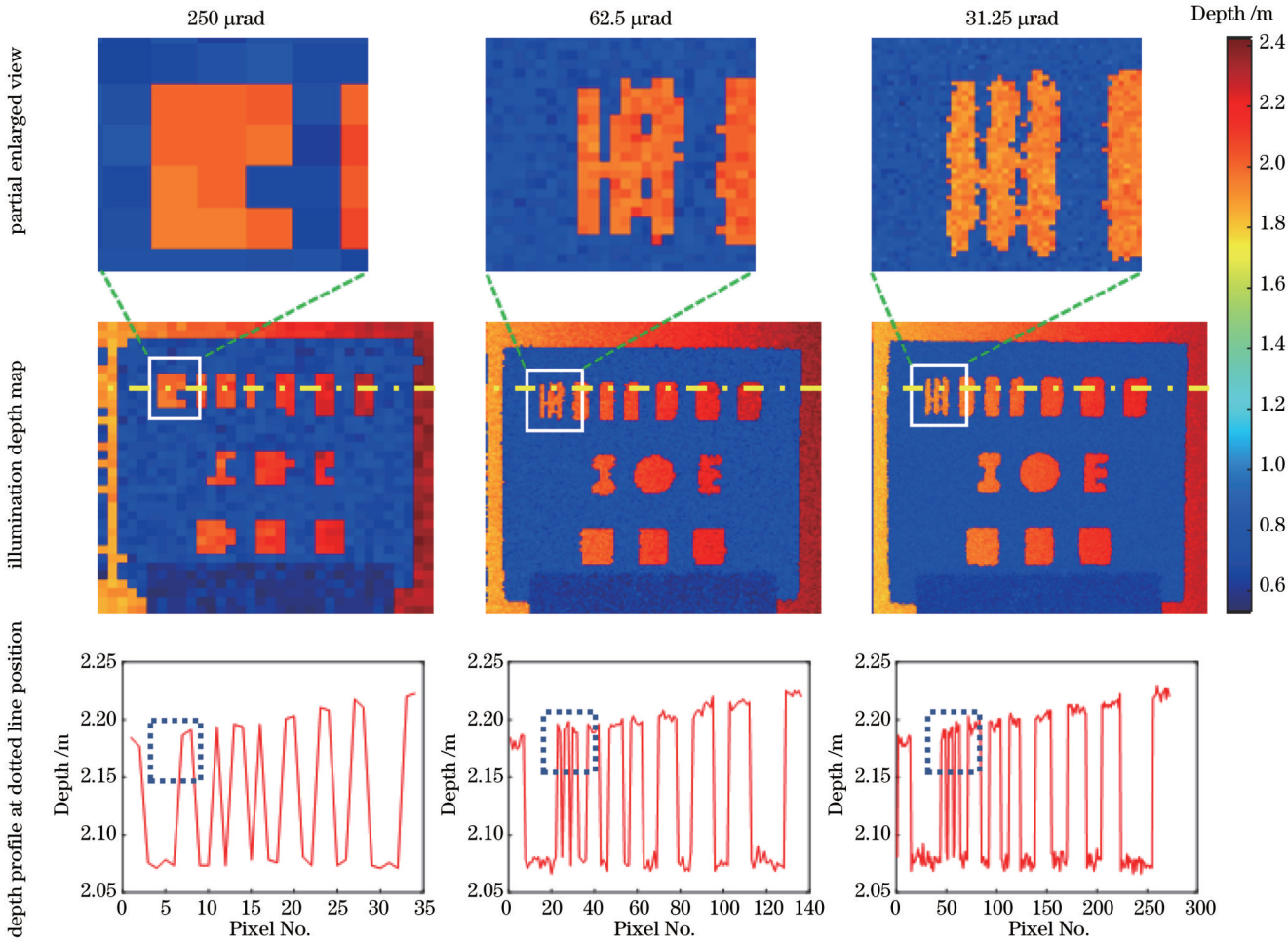

图 7　10 m 处聚焦光束照明时不同扫描步长下的深度图

Fig. 7　Illumination depth maps of focused beam with different scanning steps at 10 m

大图，第三行为第二行虚线位置深度剖面图。随着扫描精细度的增加，0.9 mm缝由无法分辨到粗略分辨再到清晰分辨。

此外，对曲线峰值进行拟合，由斜率算得倾斜角为35.0°，非常接近33.3°，验证了系统的高深度精度。出现偏差的原因一方面是系统误差，另一方面则是出射光束没有完全与透射式分辨率靶垂直。从缝的边缘可以看到，亚像素扫描可在一定程度上降低多重回波的影响。

4.2　熊猫玩偶

系统亚厘米级的深度分辨率保证了低落差目标能被精确成像。为了进一步验证亚像素扫描技术的超分辨能力，对放置在距发射端8 m处的熊猫玩偶采用聚焦照明进行探测，其中接收视场角为250 μrad。图8第一行为强度图，第二行为深度图，可以看到，随着扫描步长的减小，玩偶周围的锯齿迅速减少，轮廓更为平滑和准确。图8第三行是第二行虚线位置的剖面深度图，其中深度差 d_B-d_A=1545.6 mm−1538.4 mm=7.2 mm、深度差 d_D-d_C=1540.8 mm−1536.0 mm=4.8 mm、深度差 d_F-d_E=1545.6 mm −1536.0 mm=9.6 mm。由深度差可知，熊猫边缘深度抖动与系统时间抖动相匹配，达到亚厘米级。亚像素扫描虽然能使目标轮廓更为清晰，但相比于逐像素扫描，其在深度估计上的提升效果并不明显。

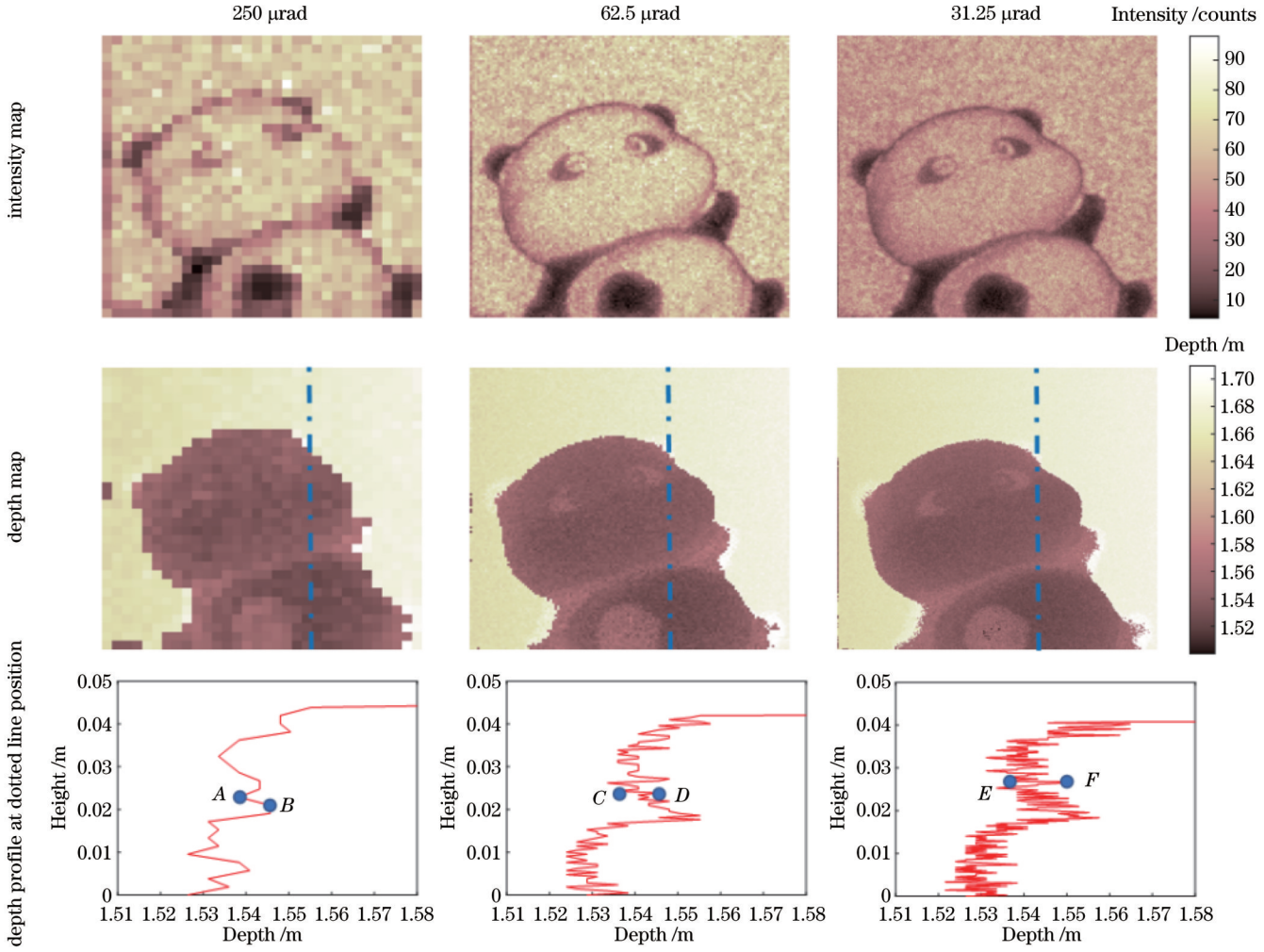

图8　8 m处聚焦光束照明熊猫玩偶时的强度图和深度图

Fig. 8　Intensity and depth maps of panda doll illuminated by focused beam at 8 m

为了更直观地观察亚像素扫描对成像分辨率的改进效果，重建了熊猫三维轮廓，如图9所示。结果表明，亚像素扫描能使目标成像更为清晰、准确。如上所述，这些结果都是通过简单的计算获得，如果构建更精细的传播模型，利用像素间的空间相关性进行互相关处理，再融合高分辨率的强度图和深度图[30]，可进一步改善成像结果。

5　结　　论

通过实验验证了使用准直光束和聚焦光束照明的亚像素扫描超分辨技术。透射式分辨率靶的成像结果表明，在相同的FoV下，采用小光斑照明能有效提高成像分辨率，而使用亚像素扫描获得的重建图像比逐像素扫描图像更为平滑、清晰，横向分辨率由准直照明

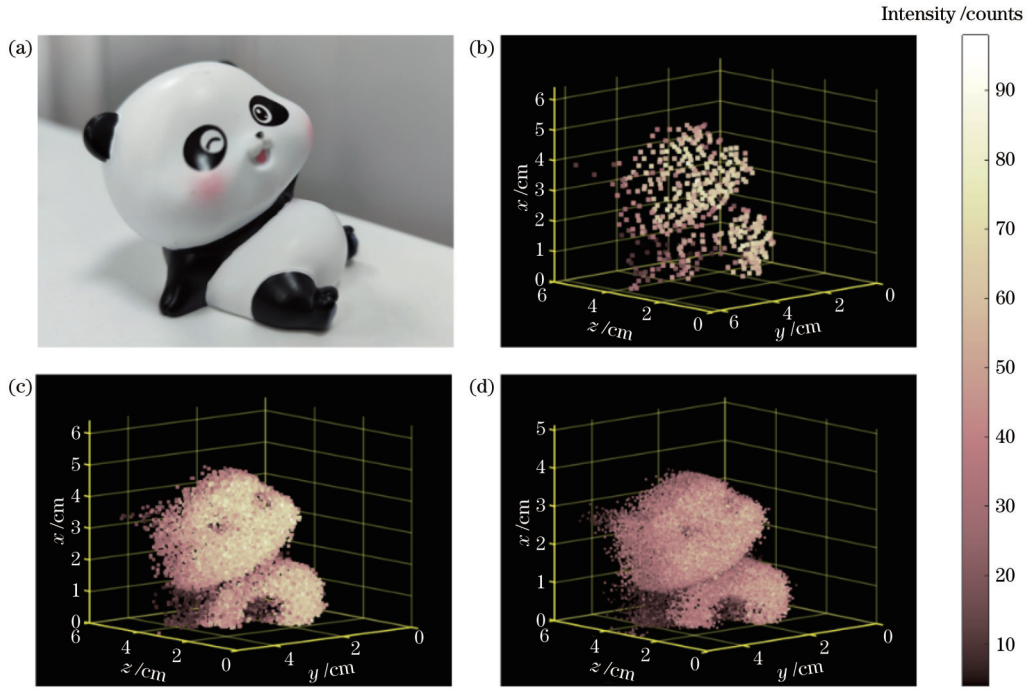

图 9　熊猫玩偶的三维重建结果。(a)实物;(b)逐像素扫描结果;(c) 1/4 亚像素扫描结果;(d) 1/8 亚像素扫描结果

Fig. 9　3D reconstruction results of panda doll. (a) Picture of panda doll; (b) result of pixel by pixel scanning; (c) result of 1/4 sub-pixel scanning; (d) result of 1/8 sub-pixel scanning

逐像素扫描的 5.0 mm 提高到聚焦照明亚像素扫描的 0.9 mm,实现了超光学系统衍射极限成像。此外,在激光雷达系统中,亚像素扫描对分辨率的提升效果也与光斑大小有关。受限于系统的扫描精度和扫描时间,无限制地降低扫描步长显然是不现实的,需要根据自身系统,综合考虑测量时间、需求分辨率和系统极限来选择亚像素扫描步长。针对采集时间长的问题,可先用大步长扫描快速寻找目标,再对感兴趣的区域进行亚像素扫描。后续场外实验时,可利用贝塞尔光束一定程度上抗大气湍流[31]、烟雾[32]等能力和超振荡光束超衍射极限中心光斑[33],加入先进算法,结合小光斑照明和亚像素扫描的优势,进一步提高系统成像分辨率。总而言之,小光斑照明、亚像素扫描技术在远距离激光雷达提高空间分辨率方面具有巨大潜力。现有激光雷达较少从光束调制手段方面入手,尤其是针对散射目标,矢量聚焦照明光场有望实现更高分辨率的激光雷达和非视域成像[34]。

参　考　文　献

[1] Swatantran A, Tang H, Barrett T, et al. Rapid, high-resolution forest structure and terrain mapping over large areas using single photon lidar[J]. Scientific Reports, 2016, 6: 28277.

[2] Degnan J J, Field C T. Moderate to high altitude, single photon sensitive, 3D imaging lidars[J]. Proceedings of SPIE, 2014, 9114: 91140H.

[3] Buyukdemircioglu M, Kocaman S. Reconstruction and efficient visualization of heterogeneous 3D city models[J]. Remote Sensing, 2020, 12(13): 2128.

[4] Bagheri H, Schmitt M, Zhu X X. Fusion of multi-sensor-derived heights and OSM-derived building footprints for urban 3D reconstruction[J]. ISPRS International Journal of Geo-Information, 2019, 8(4): 193.

[5] Yi S, Min S. A practical calibration method for stripe laser imaging system[J]. IEEE Transactions on Instrumentation and Measurement, 2021, 70: 5003307.

[6] Harmatys W, Gąska A, Gąska P, et al. Assessment of background illumination influence on accuracy of measurements performed on optical coordinate measuring machine equipped with video probe[J]. Sensors, 2021, 21(7): 2509.

[7] Du P F, Zhang F, Li Z P, et al. Single-photon detection approach for autonomous vehicles sensing[J]. IEEE Transactions on Vehicular Technology, 2020, 69(6): 6067-6078.

[8] Riemensberger J, Lukashchuk A, Karpov M, et al. Massively parallel coherent laser ranging using a soliton microcomb[J]. Nature, 2020, 581(7807): 164-170.

[9] Marino R M, Davis W R. Jigsaw: a foliage-penetrating 3D imaging laser radar system[J]. Lincoln Laboratory Journal, 2005, 15(1): 23-36.

[10] Huang G H, Shu R, Hou L B, et al. Design and performance of a fiber array coupled multi-channel photon counting, 3D imaging, airborne lidar system[J]. Proceedings of SPIE, 2014, 9080: 90800F.

[11] Kirmani A, Venkatraman D, Shin D, et al. First-photon imaging[J]. Science, 2014, 343(6166): 58-61.

[12] Pawlikowska A M, Halimi A, Lamb R A, et al. Single-photon three-dimensional imaging at up to 10 kilometers range[J]. Optics Express, 2017, 25(10): 11919-11931.

[13] Li Z P, Ye J T, Huang X, et al. Single-photon imaging over 200 km[J]. Optica, 2021, 8(3): 344-349.

[14] Li Z H, Wu E, Pang C K, et al. Multi-beam single-photon-counting three-dimensional imaging lidar[J]. Optics Express, 2017, 25(9): 10189-10195.

[15] McCarthy A, Collins R J, Krichel N J, et al. Long-range time-of-flight scanning sensor based on high-speed time-correlated single-photon counting[J]. Applied Optics, 2009, 48(32): 6241-6251.

[16] Li Z P, Huang X, Cao Y, et al. Single-photon computational

3D imaging at 45 km[J]. Photonics Research, 2020, 8(9): 1532-1540.
[17] Gao L, Shao L, Higgins C D, et al. Noninvasive imaging beyond the diffraction limit of 3D dynamics in thickly fluorescent specimens[J]. Cell, 2012, 151(6): 1370-1385.
[18] Singh B K, Nagar H, Roichman Y, et al. Particle manipulation beyond the diffraction limit using structured super-oscillating light beams[J]. Light: Science & Applications, 2017, 6(9): e17050.
[19] Perinchery S M, Haridas A, Shinde A, et al. Breaking diffraction limit of far-field imaging via structured illumination Bessel beam microscope (SIBM)[J]. Optics Express, 2019, 27(5): 6068-6082.
[20] Li Z P, Huang X, Jiang P Y, et al. Super-resolution single-photon imaging at 8.2 kilometers[J]. Optics Express, 2020, 28(3): 4076-4087.
[21] Xue R K, Kang Y, Zhang T Y, et al. Sub-pixel scanning high-resolution panoramic 3D imaging based on a SPAD array[J]. IEEE Photonics Journal, 2021, 13(4): 3900106.
[22] 郭静菁, 费晓燕, 葛鹏, 等. 基于全光纤光子计数激光雷达的高分辨率三维成像[J]. 红外与激光工程, 2021, 50(7): 20210162.
Guo J J, Fei X Y, Ge P, et al. High-resolution three-dimensional imaging based on all-fiber photon-counting Lidar system[J]. Infrared and Laser Engineering, 2021, 50(7): 20210162.
[23] Park S C, Park M K, Kang M G. Super-resolution image reconstruction: a technical overview[J]. IEEE Signal Processing Magazine, 2003, 20(3): 21-36.
[24] Zheng G A, Lee S A, Yang S, et al. Sub-pixel resolving optofluidic microscope for on-chip cell imaging[J]. Lab on a Chip, 2010, 10(22): 3125-3129.
[25] Ling F, Du Y, Xiao F, et al. Super-resolution land-cover mapping using multiple sub-pixel shifted remotely sensed images[J]. International Journal of Remote Sensing, 2010, 31(19): 5023-5040.
[26] Lin W Y, Panusopone K, Baylon D M, et al. A fast sub-pixel motion estimation algorithm for H.264/AVC video coding[J]. IEEE Transactions on Circuits and Systems for Video Technology, 2011, 21(2): 237-242.
[27] Murn L, Smeaton A F, Mrak M. Interpreting super-resolution CNNs for sub-pixel motion compensation in video coding[C]// Proceedings of the 29th ACM International Conference on Multimedia, October 20-24, 2021, Virtual Event, China. New York: ACM Press, 2021: 3803-3806.
[28] Yin W Y, He W J, Gu G H, et al. Approach for LIDAR signals with multiple returns[J]. Applied Optics, 2014, 53(30): 6963-6969.
[29] Shin D, Xu F H, Wong F N C, et al. Computational multi-depth single-photon imaging[J]. Optics Express, 2016, 24(3): 1873-1888.
[30] Gyongy I, Hutchings S W, Halimi A, et al. High-speed 3D sensing via hybrid-mode imaging and guided upsampling[J]. Optica, 2020, 7(10): 1253-1260.
[31] Meyers R E, Deacon K S, Tunick A D, et al. Virtual ghost imaging through turbulence and obscurants using Bessel beam illumination[J]. Applied Physics Letters, 2012, 100(6): 061126.
[32] Shi H T, Shen G Y, Qi H Y, et al. Noise-tolerant Bessel-beam single-photon imaging in fog[J]. Optics Express, 2022, 30(7): 12061-12068.
[33] Zheludev N I, Yuan G H. Optical superoscillation technologies beyond the diffraction limit[J]. Nature Reviews Physics, 2022, 4(1): 16-32.
[34] Cao R Z, de Goumoens F, Blochet B, et al. High-resolution non-line-of-sight imaging employing active focusing[J]. Nature Photonics, 2022, 16(6): 462-468.

High Resolution 3D Imaging Based on Confocal Sub-Pixel Scanning

Huang Yuanjian[1,2], Li Xiaoyin[1,2], Ye Wenyi[1,2], Guo Yinghui[1,2], Yang Longfei[3], He Jiang[3], Ke Yuan[3], Pu Mingbo[1,2], Luo Xiangang[1,2*]

[1]*State Key Lab of Optical Technologies on Nano-Fabrication and Micro-Engineering, Institute of Optics and Electronics, Chinese Academy of Sciences, Chengdu* 610209, *Sichuan, China*;

[2]*School of Electronic, Electrical and Communication Engineering, University of Chinese Academy of Sciences, Beijing* 101408, *China*;

[3]*Tianfu Xinglong Lake Laboratory, Chengdu* 610299, *Sichuan, China*

Abstract

Objective Lidar is widely applied in 3D imaging because of its high precision, high resolution, and long working distance. The size and distribution of the illumination spot on the imaging target are important factors affecting the imaging resolution. The smaller spot size results in finer information obtained on the target surface and clearer 3D information of the reconstructed object. The increase in spot size affects the quality of laser scanning 3D imaging mainly in two aspects. On one hand, it will reduce the energy of light signals shining on the surface of the object, thereby leading to weakening return light signals and affecting the detection distance. On the other hand, the area of large light spot shining on the object surface is also large, which causes multiple echo signals generated by the same light spot due to the change of object surface, thus affecting the ranging accuracy. However, most of the existing lidars employ collimated Gaussian beams to emit. When imaging at a long distance, the spatial resolution is significantly reduced with the increasing target distance due to the laser divergence angle and the diffraction limit of the optical system. To this end, this paper improves the system resolution from the aspect of output beam control and scanning mode.

Methods In laser scanning 3D imaging, the beam scans and illuminates the target point by point, and detects the return light signals at different positions of the target to obtain the depth information of the detection target surface and realize 3D imaging. In this process, the traditional laser scanning 3D imaging generally irradiates the laser collimated and expanded to a distant target object in a parallel beam mode for reducing the divergence of beams. The size of the light spot at the target object mainly depends on the divergence angle of the beam after expansion and the imaging working distance and is generally far greater than that of the light spot under the diffraction limit. By changing the focal length of the system, this paper focuses the light spot at the imaging target to obtain a small light spot. Sub-pixel scanning is originally proposed as a method to obtain high-resolution (HR) images from multiple low-resolution (LR) images for ordinary digital cameras. In sub-pixel scanning technology, the basic premise to improve spatial resolution is to capture multiple LR images from the same scene. LR images are subsampled (aliased) and shifted with sub-pixel accuracy. If the LR image is shifted in integer units, each image contains the same information, so there is no new information available to reconstruct the HR image. However, if LR images have different sub-pixel offsets from each other and there is aliasing, HR images can be obtained using the new information contained in each LR image. As an analogy to lidar, sub-pixel scanning can also be employed to enhance the imaging resolution of the system.

Results and Discussions A confocal sub-pixel scanning photon counting lidar is designed to improve the spatial resolution of the system. The size of the focused spot at 10 m is about 1/4 of that of the collimated spot. Compared with pixel-by-pixel scanning, 1/8 sub-pixel scanning at 7 m and 10 m can recover the letter I on the resolution target (Fig. 4). Focused lighting can effectively enhance echo energy (Fig. 5) and imaging resolution (Fig. 6) compared with collimated lighting. Combined with sub-pixel scanning, the imaging resolution of the system is increased from 5.0 mm to 0.9 mm, which exceeds the diffraction limit of the system. In addition, with the decreasing sub-pixel scanning step, the imaging resolution will also be improved. The experimental results show that through sub-pixel scanning, the aliasing of the reconstructed image is rapidly reduced, and the contour is smoother and more accurate (Fig. 8).

Conclusions This paper demonstrates the sub-pixel scanning high-resolution technology using collimated and focused illumination through experiments. The imaging results of the transmissivity resolution target show that under the same FoV, small spot illumination can effectively improve the imaging resolution. The reconstructed image obtained by sub-pixel scanning is smoother and clearer than the pixel-by-pixel image. The horizontal resolution is increased from 5.0 mm per pixel for collimated illumination to 0.9 mm for focused illumination with sub-pixel scanning and exceeds the limit of system angular resolution. In addition, in the lidar system, the resolution improvement of sub-pixel scanning is also related to the spot size. Small spot illumination and sub-pixel scanning technology have great potential in improving the spatial resolution of long-range lidar.

Key words optical design; lidar; sub-pixel scanning; confocal illumination; high resolution

Vol. 43, No. 8/April 2023/Acta Optica Sinica | Research Article·English Version

ACTA OPTICA SINICA

High-Resolution 3D Imaging Based on Confocal Sub-Pixel Scanning

Huang Yuanjian[1,2], Li Xiaoyin[1,2], Ye Wenyi[1,2], Guo Yinghui[1,2], Yang Longfei[3], He Jiang[3], Ke Yuan[3], Pu Mingbo[1,2], Luo Xiangang[1,2]

[1]*State Key Laboratory of Optical Technologies on Nano-Fabrication and Micro-Engineering, Institute of Optics and Electronics, Chinese Academy of Sciences, Chengdu* 610209, *Sichuan, China*;

[2]*School of Electronic, Electrical and Communication Engineering, University of Chinese Academy of Sciences, Beijing* 101408, *China*;

[3]*Tianfu Xinglong Lake Laboratory, Chengdu* 610299, *Sichuan, China*

Abstract Lidar technology is widely used for three-dimensional imaging owing to its high precision, resolution, and long operating range. However, owing to the diffraction limit of optical systems, the spatial resolution of lidar decreases significantly as the target distance increases. In this paper, we propose a high-resolution photon-counting lidar based on confocal illumination and sub-pixel scanning technology. A 10-m imaging experiment was conducted in a laboratory to verify the proposed system. The results show that, compared with collimated illumination, confocal illumination can increase the system′s spatial resolution from 5.0 to 0.9 mm, which not only exceeds the diffraction limit of the optical system but also effectively reduces the impact of multi-path reflections and enhances the intensity of the return signal.

Key words optical design; lidar; sub-pixel scanning; confocal illumination; high resolution

CLC number TN958.98 **Document code** A **DOI:** 10.3788/AOS221974

1 Introduction

Light detection and ranging (lidar) is an active optical three-dimensional (3D) imaging technology that uses pulsed or continuous lasers as light sources. Its operating principle is such that a laser beam is emitted toward a target, and then parameters such as the arrival time and strength of the reflected or scattered signal are measured to determine the distance, azimuth, motion state, and surface optical characteristics of the target, thereby establishing the 3D imaging information of the measured target. Lidar has wide applications and prospects in various fields such as terrain mapping[1,2], city modeling[3,4], industrial manufacturing[5,6], and autonomous driving[7,8].

With the continuous expansion of the application range of lidar, the demand for lidar continues to increase, and long-range high-precision laser 3D imaging has become a research focus internationally, and extensive research has been conducted in this area. For example, in 2005, a 32×32 Geiger-mode avalanche photodiode array was used to achieve a resolution of 40 cm at 150 m[9], and vehicles hidden under camouflage nets and tree leaves were recovered. In 2013, a multi-channel scanning single-photon lidar was used to assist in the soft landing of "Chang′e 3" on the moon[10], achieving a detection accuracy of less than 0.2 m. In 2014, Kirmani *et al.* achieved a high-resolution 3D reconstruction of a human model by utilizing spatial correlation in actual scenes and the physical characteristics of low-flux measurements, with each pixel receiving only a single photon[11]. In 2017, an indium gallium arsenide single-photon detector combined with a total variation optimization algorithm was used to recover a 38° slope at a distance of 10.5 km[12]. In 2021, Li *et al.* built a 1550 nm photon-counting lidar system that utilized efficient noise-suppression techniques such as time gating and matching the field of view (FoV) of the detector with the beam divergence angle to achieve precise mountain peak imaging at a distance of 201.5 km[13]. However, owing to the diffraction limit, the spatial resolution decreases significantly as the imaging distance extends to the kilometer range.

Reducing the size of the laser spot at the target is an effective method of improving the imaging resolution, and it has been widely used in fields such as microscopy. For example, in 2012, Gao *et al.* of the Howard Hughes Medical Institute used a Bessel beam to achieve fast 3D imaging of living samples beyond the diffraction limit[14]. In 2017, Single *et al.* from the Technion Israel Institute of Technology used super-

oscillatory beams to achieve a positioning accuracy far beyond the standard diffraction limit for high-resolution capture[15]. In 2019, Perinchery *et al*. from Nanyang Technological University successfully imaged a 0.2 μm fluorescent bead using a Bessel beam microscopy system, achieving sub-Airy resolution imaging [16]. The core concept of these methods is to reduce the size of the laser spot. Although single-photon lidar has enabled significant breakthroughs in imaging distance, most reported systems[17-19] use collimated Gaussian beams for laser emission. When the imaging distance reaches a kilometer or even hundreds of kilometers, the spatial resolution sharply decreases owing to the laser divergence angle.

In addition, sub-pixel scanning provides a relatively simple method for improving the resolution of single-photon lidar. By controlling the scan-step size at the single-pixel scale, a series of low-resolution images can be captured and combined into higher-resolution images using a computational method. For example, in 2020, Li *et al*. designed a single-photon lidar based on sub-pixel scanning, achieving a resolution of 5 cm at a distance of 8.2 km[20]. In 2021, Xue *et al*. used sub-pixel scanning to increase the spatial resolution from 3 to 0.33 mm at a distance of 3 m[21]. Guo *et al*. used a multi-distance reconstruction algorithm with sub-pixel scanning and adaptive noise threshold to achieve target imaging at 3.1 km with a spatial resolution of 0.11 m[22].

To address the limitations of imaging resolution in lidar, we designed a variable-focus photon-counting lidar operating at 1550 nm in this study, combining the advantages of small-spot illumination and sub-pixel scanning. Demonstration experiments were conducted indoors, and multiple echo waves were effectively reduced by focusing illumination, achieving a slit imaging of 0.9 mm at 10 m and a spatial resolution exceeding the diffraction limit.

2 Scheme design

2.1 3D laser scanning imaging

In 3D laser scanning imaging, the beam is used to scan and illuminate the target point-by-point, and the depth information of the surface of the target is obtained by detecting the return light signal at different locations on the target to obtain the required 3D imaging. In this process, the size and distribution of the illumination spot on the imaging target are important factors that affect the imaging resolution. The smaller the spot size, the finer the information obtained on the target surface and the clearer the 3D information of the reconstructed object. In traditional 3D laser scanning imaging, to reduce beam divergence, the laser is generally collimated and expanded to illuminate the far target object in a parallel beam mode. The size of the spot on the target object depends primarily on the divergence angle of the expanded beam and the imaging working distance, which is frequently much larger than the spot size below the diffraction limit. The increase in spot size primarily affects the quality of 3D laser scanning imaging in two ways: on one hand, it reduces the energy of the light signal illuminating the surface of the object, leading to weaker return light signals and affecting the detection distance; on the other hand, the large spot size illuminating the surface of the object leads to multiple echo signals owing to the changes in the object surface shape, which affects the ranging accuracy. To achieve long-range high-resolution 3D imaging to solve the above problems, we propose a 3D imaging method based on confocal scanning, as shown in Figure 1, which replaces parallel illumination beams with focused illumination beams and uses the characteristics of confocal scanning to essentially match the receiver and emitter FoV, ensuring scanning accuracy while reducing echo noise.

The resolution of an imaging system is limited by the optical diffraction limit, which primarily depends on the aperture of the optical system. To reduce the beam divergence for parallel illumination beams, we must increase the waist of the beam, which requires the use of an optical system with a large aperture for beam transmission and reception. The size of the parallel illumination spot primarily depends on the size of the emission spot (D), divergence angle of the beam (θ), and working distance (L); the formula for calculating the spot size at the target is given in Equation (1). Assuming a long-range imaging scene of 10 km, D of 300 mm, and θ of 35 μrad, the spot diameter at the target can be calculated using Equation (1), where $D_{\text{target 1}} \approx 650$ mm.

$$D_{\text{target 1}} \approx D + L \times \tan\theta \approx D + L \times \theta. \quad (1)$$

For focused illumination, the size of the focused spot can be approximated using the diffraction limit formula in Equation (2), which primarily depends on D, the laser wavelength (λ), and L. As shown in Figure 1(b), the spot can be focused on the surface of the object by changing the distance between the lenses

(d) using the formula of light focal length ($\Phi=\frac{1}{f}$, the reciprocal of the focal length): $\Phi=\Phi_1+\Phi_2-d\Phi_1\Phi_2$. Therefore, illumination with near-diffraction-limit scale can be achieved in the focal-depth range. For collimated illumination at the target, the spot size is approximately 5.1 times larger than that of focused beam illumination when $L=10$ km, $D=300$ mm, and $\lambda=1550$ nm are substituted into Equation (2); $D_{\text{target 2}}\approx 126$ mm.

$$D_{\text{target 2}}\approx\frac{2.44\lambda}{D}\times L. \tag{2}$$

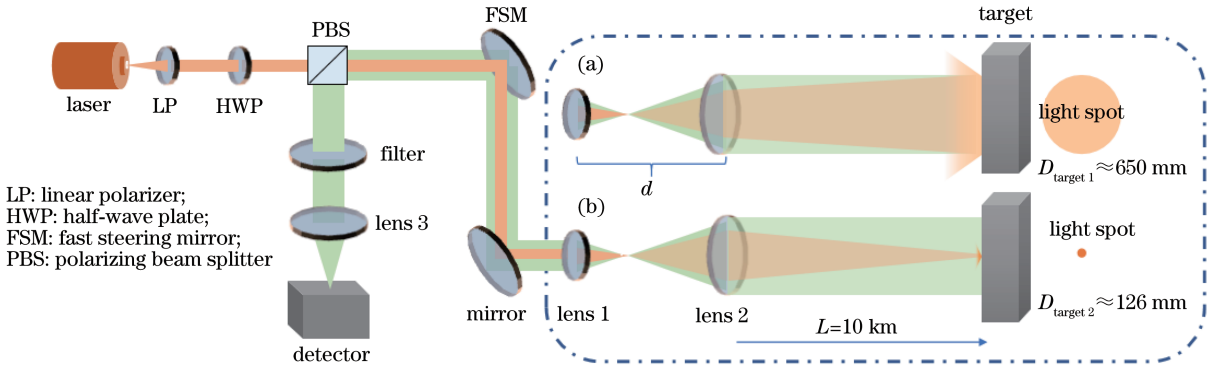

Fig. 1 Schematic of laser 3D imaging under different illumination modes. (a) Collimated illumination; (b) focused illumination

2.2 Sub-pixel scanning super-resolution method

Sub-pixel scanning was originally proposed for obtaining high-resolution (HR) images from multiple low-resolution (LR) images captured from the same scene using an ordinary digital camera [23] and has been widely used in fields such as medical imaging[24], satellite imaging[25] and video[26, 27]. In sub-pixel scanning technology, the basic premise of improving the spatial resolution rate involves obtaining multiple LR images for the same scene with a finer step size, smaller than the minimum pixel pitch, and obtaining more image detail information through overlapping sampling between pixels. The LR images are subsampled and shifted at sub-pixel accuracy. If the LR images are shifted in pixel-pitch integer units, each image contains the same information, and no new information is available to reconstruct the HR image.

In lidar, the FoV of single-point detection is equivalent to a size of one pixel. To balance the detection efficiency and reduce the environmental background noise, the system's FoV angle is frequently slightly smaller than the laser divergence angle, which means that pixel-by-pixel scanning refers to a scan step size equal to the FoV, whereas sub-pixel scanning refers to a scan step size smaller than the FoV. After multiple frames of LR images are obtained, the key aspect of sub-pixel scanning super-resolution technology is the arrangement and sorting of the composite images and extraction of more detailed information from the overlapping parts of multiple LR images. In Figure 2, a picture is composed of 3×3 grid units, the system simulation detection FoV covers 2×2 grid units, and the system scan step is one grid unit (*i. e.*, 1/2 FoV step size sub-pixel scanning). The numbers marked below each image indicate the order of the sub-pixel scanning. A 1/2 sub-pixel scanning is performed for the position (1 2 4 5) of 1, and the target pixel is changed from 2×2 (LR) to 4×4 (HR). For a single-point laser radar, the scan process requires only to be sorted in order.

3 Experimental device

The experimental setup is shown In Figure 3. A coaxial design and time-correlated single photon counting (TCSPC) were adopted. TCSPC technology can effectively reduce random errors and obtain accurate time information by dividing the different flight times into discrete time grids and integrating the response in the form of a histogram to discern photon signals. The system used a fiber laser with a wavelength of 1550 nm, which generated a laser pulse width of 2.315 ps at a repetition rate of 12.7 MHz. The 1550 nm operating band has the advantages of eye safety, low solar background noise, and low atmospheric loss, which were beneficial for subsequent off-site experiments. The laser beam was 2.0 mm in diameter and had a divergence angle of 1.0 mrad through the collimator. After 10 beam expansions, it passed through a polarization beam splitter in the direction of horizontal polarization, and then it was

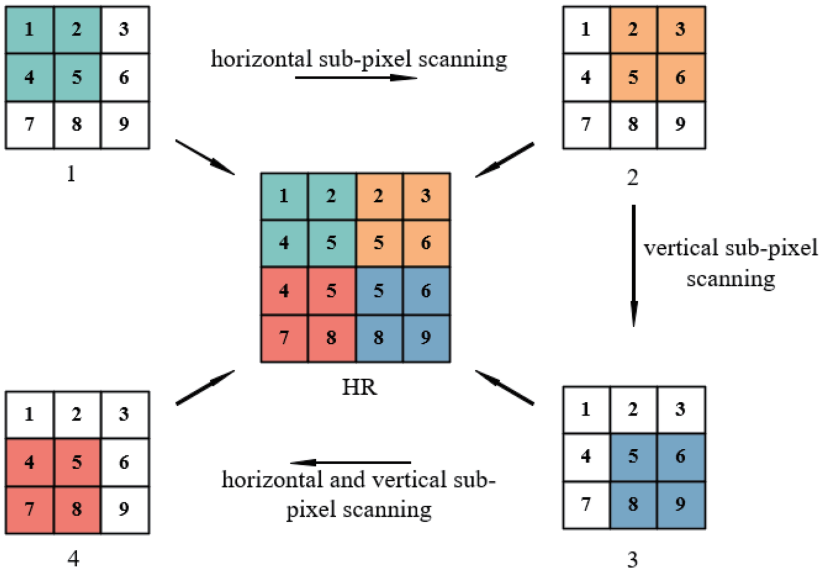

Fig. 2 Schematic of pixel points layout under sub-pixel scanning

projected to the target through a fast mirror and 2× telescope. The collimation and focusing illumination modes were switched by adjusting the distance between the telescope objective and eyepiece. When collimated, the beam did not pass through the 10× expansion; thus, after passing through the telescope, the divergence angle became 0.5 mrad.

Table 1 lists the system parameters. Compared with single-mode fiber, a multi-mode fiber with a diameter of $D=50\ \mu m$ was adopted for the detector, which effectively improved the coupling of echo photons while limiting the FoV. The coupling lens focal length was $f=100$ mm, and the equivalent focal length when the beam was collimated and focused was $f\approx 200$ mm; therefore, the system's reception FoV was $2\times\arctan[D/(2f)]=250\ \mu rad$. As shown in Figure 3, both the laser and single photon detector (SPAD) were connected to the transmitting and receiving optical paths through fiber jumpers. Therefore, the optical fiber laser, SPAD, and fibers with different diameters could be replaced flexibly during the experiment to satisfy different experimental requirements. The scanning repetition accuracy of the fast mirror (Newport, FSM300) was less than 3 μrad to ensure the sub-pixel scanning capability. The drive signal of FSM300 was provided using a PLC (SIMATIC S7-1200), which was controlled using a computer software program written in LabVIEW. A reflective diffuser (DG10-1500-P01, Thorlabs) was placed at 1 m, and the time jitter of the system was measured at 48 ps with an equivalent ranging accuracy of 7.2 mm, reaching a sub-centimeter resolution. Time jitter primarily resulted from the detector response time jitter, laser source jitter and laser pulse width, timing circuit jitter, and jitter from the equipment and other instruments.

Table 1 Parameters of the confocal lidar system

Parameter	Value
Wavelength /nm	1550
Laser pulse width /ps	2.315
Laser repetition rate /MHz	12.7
FoV of the detector /μrad	250
Collection fiber /μm	50
Scanning resolution /μrad	3
System time jitter /ps	48

Owing to the rough characteristics of the surface of the natural imaging target, the reflection is similar to diffuse reflection, which can significantly change the polarization state of the back wave light. When the roughness is sufficiently large, the reflected light completely degenerates from horizontal to random polarization. Ideally, half the polarization direction of the reflected light is orthogonal to that of the outgoing light. Although at least half of the energy is lost, the signal noise can be significantly improved by filtering the backward reflection noise.

Experiments were performed on two targets in Figure 3(b) and 3(c). Figure 3(b) shows a self-designed 3D printed resolution target with dimensions of 7.3 cm×7.3 cm. The height of all slits was 10.0 mm, and the slit widths and slit spacing in the first row from left to right were 0.9, 3.0, and 5.0 mm,

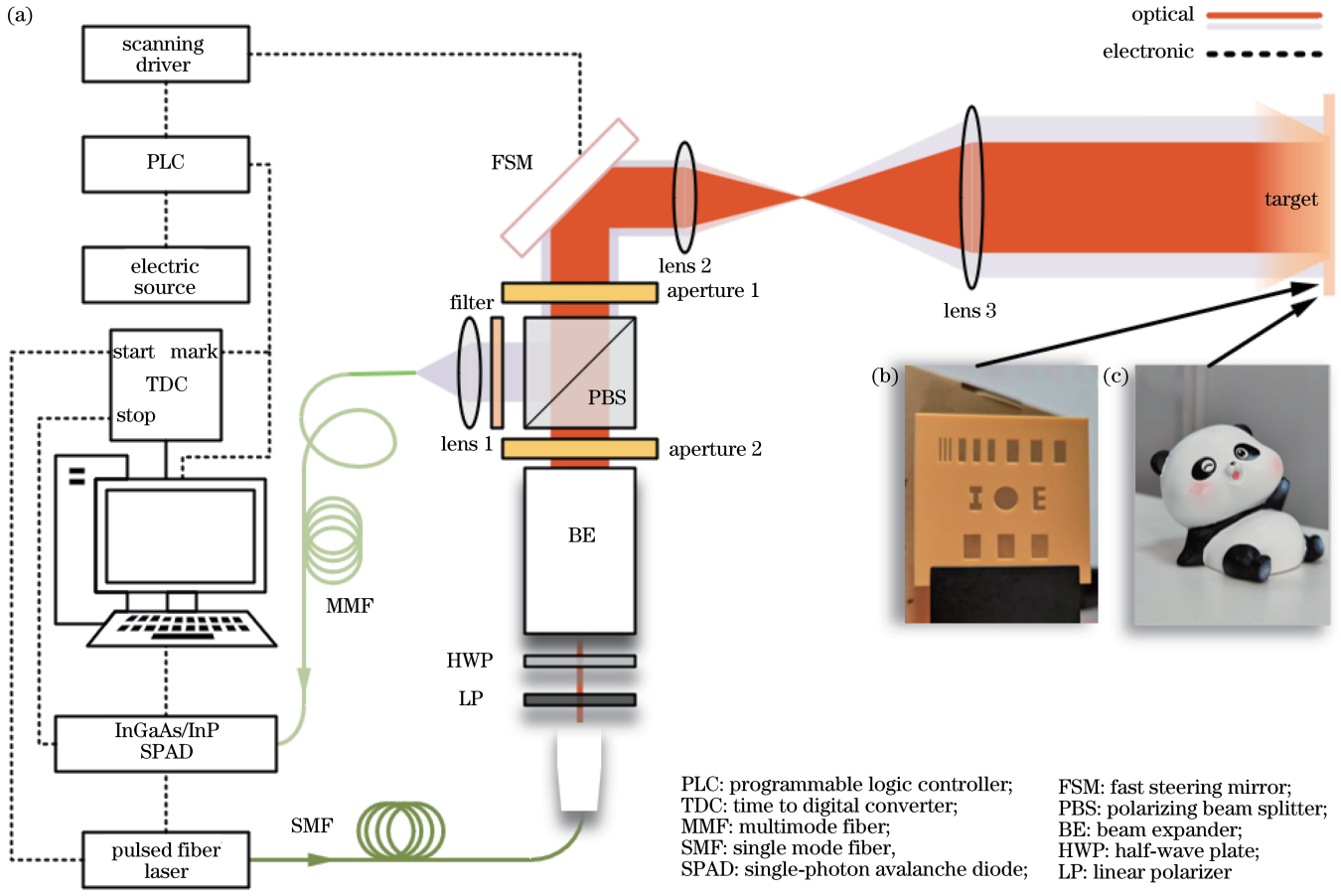

Fig. 3 Design of confocal sub-pixel scanning device. (a) Device schematic; (b) resolution target; (c) panda doll

respectively. The line widths of "I" and "E" in the middle row were 2.0 mm, and the slit width in the third row was 5.0 mm. The resolution target was primarily used to evaluate the lateral resolution of collimated and focused illumination, as well as the lateral resolution of sub-pixel scanning detection images. The second target was a panda toy with dimensions of 45.0 mm×43.5 mm×52.0 mm. When placed obliquely, the difference in the depth between the feet and nose was 18.0 mm. The panda toy was primarily used to observe the influence of the improvement in lateral resolution on depth information.

4 Experimental results and analysis

4.1 Resolution target

To characterize the lateral and longitudinal resolutions of the system quantitatively, we placed a self-made transmission resolution target at distances of 7, 8, and 10 m from the emission end, and a cardboard box was placed 15 cm behind it at an angle of 33.3°. The collimated and focused beams were scanned with step sizes of 250 μrad (per pixel), 62.50 μrad (1/4 sub-pixel), and 31.25 μrad (1/8 sub-pixel), respectively. When illuminated with a collimated beam, the spot diameters at 7, 8, and 10 m were 8.0, 8.6, and 9.5 mm, respectively. When illuminated by a focused beam, the spot diameters at 7, 8, and 10 m were 1.6, 1.8, and 2.3 mm, respectively. The single-point dwell time was 10 ms for scanning step sizes of 250 and 62.5 μrad and 5 ms for a scanning step size of 31.25 μrad. Under a synchronous signal of 12.7 MHz, the single-photon detection device was operated in a fixed gate-controlled state with a gate opening time of 6 ns and a set delay time of 10 ns to filter out the backward reflection noise and energy leaked by the polarizing beam splitter (PBS). For the depth estimation, we used a simple calculation method. First, with the response function parameters of the system instrument, we used a dual-segment Gaussian function to fit the photon histogram of each pixel, and the peak position and intensity information in the fitted curve was obtained using the maximum search algorithm.

The depth maps of the targeted illuminated resolution board at distances of 7 and 10 m for the collimated beam are shown in Figure 4. The results

demonstrate that for collimated illumination, regardless of whether sub-pixel scanning was used, the resolution of the target surface could not be accurately recovered at 7 and 10 m, and only the approximate contour was visible. Comparing the 250 μrad step scanning, the "I" contours could be recognized at 7 m, whereas at 10 m, only the "I" position with holes could be identified, which conformed to the general rule that the farther the distance, the larger the receiving surface, and the lower the imaging resolution. To understand the improvement in image quality by sub-pixel scanning, we evaluated the lateral accuracy of the same plane area as the target. The first column of Figure 4 shows the local magnification of depth information obtained using 250 and 31.25 μrad step scanning at 7 m, respectively; sub-pixel scanning with 31.25 μrad could recover the upper and lower ends of the letter "I" compared with 250 μrad scanning. Additionally, sub-pixel scanning could reconstruct smoother images than pixel-by-pixel scanning, and details could be recovered better from the completely indistinguishable letter "E" to the recognizable contour. Overall, for collimated illumination, sub-pixel scanning had limited improvement in imaging resolution, and the 0.9 mm slit could not be distinguished.

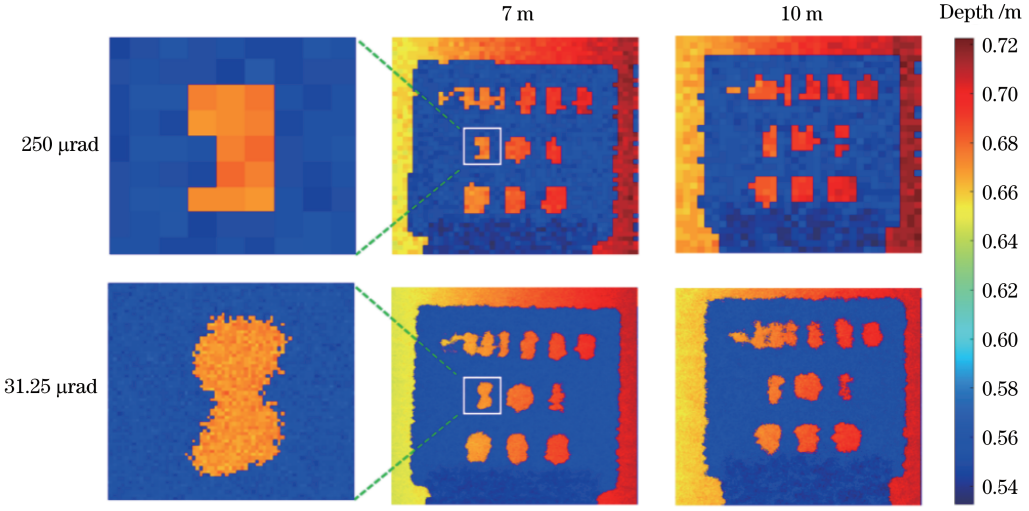

Fig. 4 Resolution target depth maps under collimated beam illumination

As shown in Figure 4, owing to the influence of multiple laser echo reflections, many burrs occurred on the transmission resolution target. Specifically, within the receiving FoV, part of the light passing through the slit irradiated the carton and illuminated the box, whereas the other light illuminates the resolution target; thus, different depth information resulted in two peaks. The intensity of the two peaks changed with the scanning movement, making it difficult to obtain accurate depth information for that position. Figure 5 shows the echo signal when the collimated beam illuminated the edge of the slit at 8 m. The first peak corresponded to the position of the resolution target at that time, and the second peak was the signal returned from the box behind the irradiated slit. When the beam moved slightly, the echo signal changed from the first peak in Figure 5(a) to the second peak in Figure 5(b), enabling us to determine whether the point belonged to the resolution target or the box behind it. Figure 5(c) shows the photon histogram obtained by measuring the diffuse reflectivity target at 8 m under the same receiving FoV angle and output power with an accumulated time of 5 s. The dashed line represents focused illumination, and the solid line represents collimated illumination. The peak value of focused illumination was approximately 3.4 times that of collimated illumination. Thus, focused illumination not only improved the system′s resolution but also significantly enhanced the detection energy.

Figure 6 shows depth images scanned pixel-by-pixel and in 1/8 sub-pixel steps using collimated and focused illumination at 8 m. The middle two columns are local magnified views of the letter "E". When pixel-by-pixel scanning was performed again, the focused illumination could accurately restore the morphology of the "E" and significantly reduce the missing and protruding parts compared with collimated illumination, indicating that small-spot illumination effectively reduced the influence of multiple reflections. In addition, when scanned with 1/8 sub-pixel steps, the

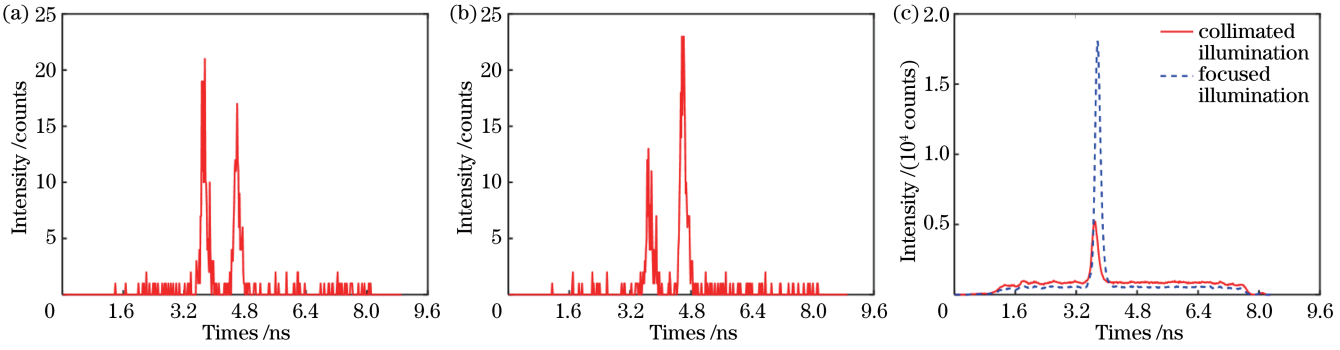

Fig. 5 Echo intensity histograms at different positions and the comparison result of intensity. (a) Histogram at the initial position; (b) histogram after a small displacement offset; (c) intensity comparison of collimating and focusing illumination

focused illumination successfully restored all the holes and the 0.9 mm slit was also clearly visible, whereas the collimated illumination could only reveal a rough outline. The results showed that sub-pixel scanning can make the imaging results more accurate and smoother but cannot significantly improve the image resolution. For multiple echoes, researchers have studied the use of algorithms for processing, such as the adaptive simulated annealing Markov chain Monte Carlo analysis method proposed by Yin *et al.* in 2014[28]. In 2016, Shine *et al.* transformed the multi-echo problem into a sparse deconvolution problem that could be solved through convex optimization[29]. This is particularly important if small light spots can be used for illumination to reduce the generation of multiple echoes from a source.

The resolution of a standard imaging system is limited by the diffraction limit, which is primarily determined by the aperture of the system. The FoV of a single detection pixel is typically set to match the diffraction limit (Airy disk diameter). Here, the angular resolution of the lidar system[20] can be calculated using $\Delta\theta = 2.44\lambda/D$. Taking our experimental setup as an example, with a laser wavelength of $\lambda = 1550$ nm, an aperture of D after aperture restriction, and a diffraction-limited resolution of approximately 158 μrad, the corresponding resolution at 8 m is approximately 1.3 mm, which is greater than 0.9 mm. Therefore, using focused laser illumination and sub-pixel scanning, the system's diffraction limit can be overcome to achieve super-resolution imaging.

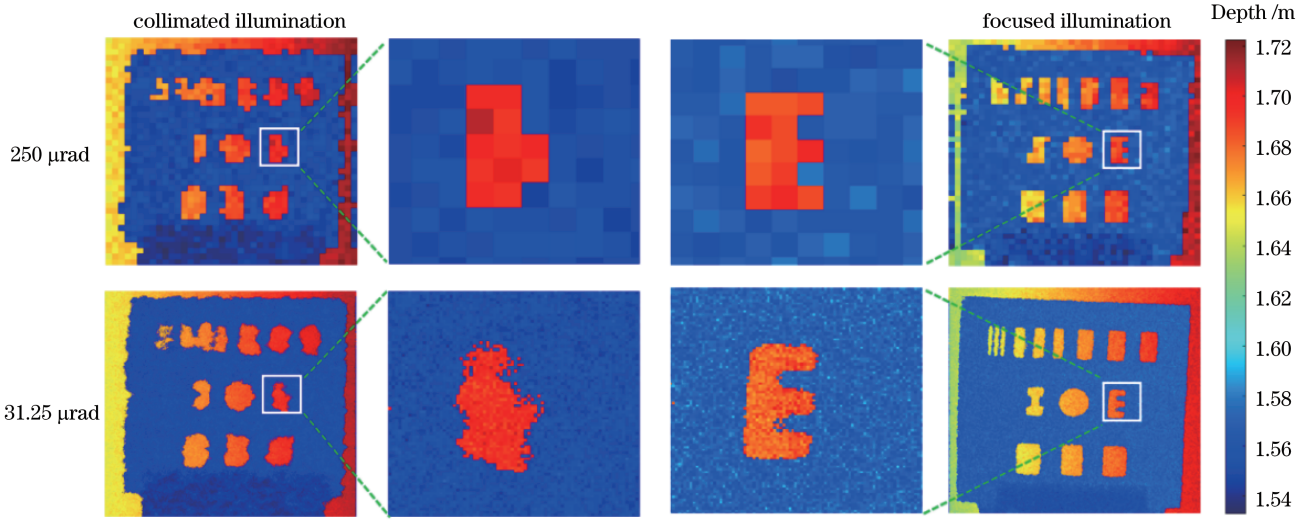

Fig. 6 Illumination depth diagrams of collimated beam and focused beam at 8 m

The effect of sub-pixel scanning at different degrees on the imaging resolution is shown in Figure 7. The first row shows a local magnified view of the 0.9 mm slit imaging results, and the third row shows the depth profile at the position of the dotted line in the second row. With the increase in scanning precision, the 0.9 mm slit progressed from being indistinguishable to roughly distinguishable and then to clearly distinguishable.

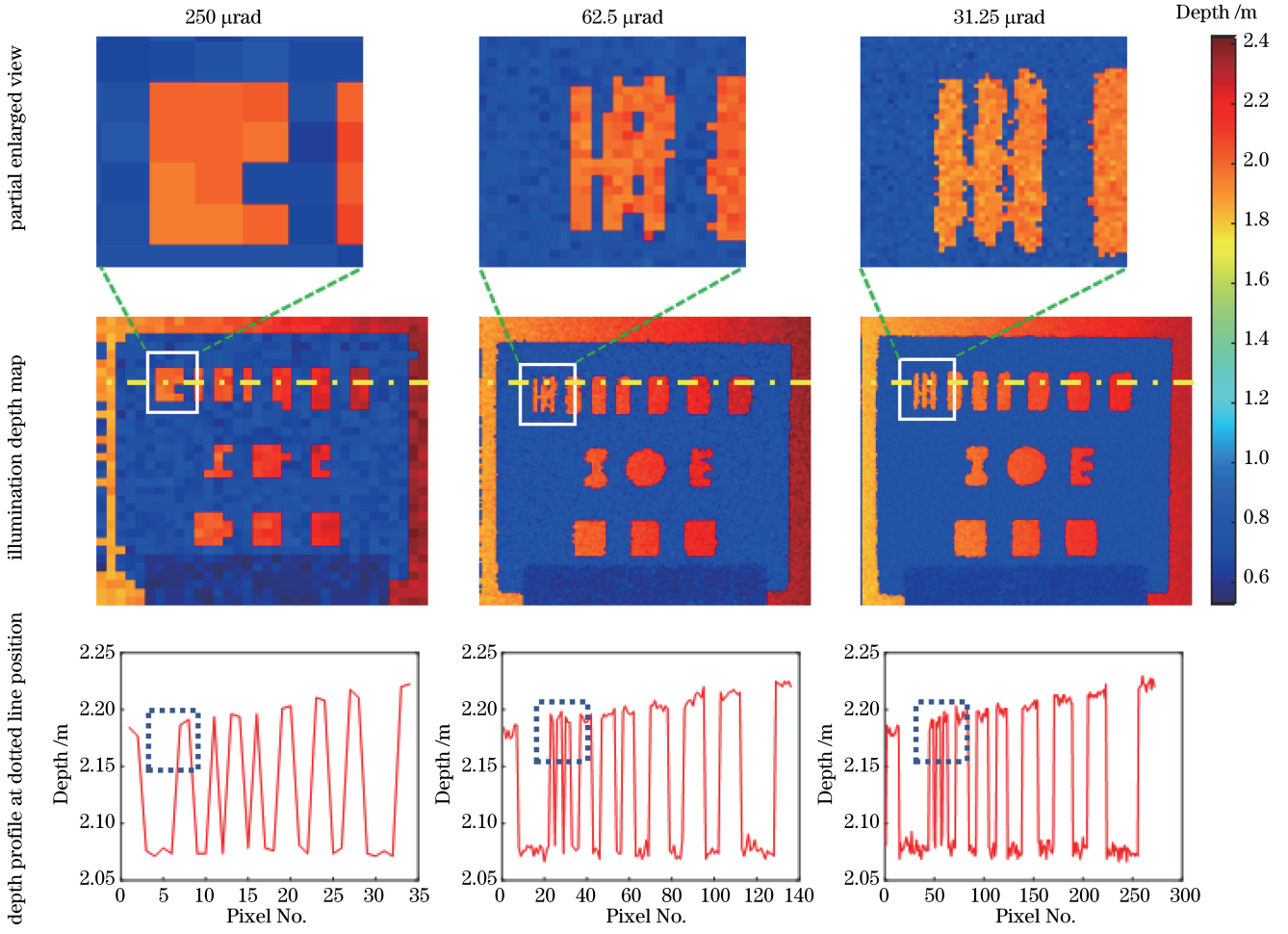

Fig. 7 Illumination depth maps of the focused beam with different scanning steps at 10 m

In addition, by fitting the peak of the curve, an inclination angle of 35.0° was calculated from the slope, which was very close to 33.3°, and verified the depth accuracy of the system. This deviation was partly due to system errors and partly because the outgoing beam was not completely perpendicular to the transmissive resolution target. From the edge of the slit, we observed that sub-pixel scanning can reduce the influence of multiple reflections to some extent.

4.2 Panda Doll

The system's sub-centimeter depth resolution ensures that targets with low height differences can be accurately imaged. To verify whether sub-pixel scanning can improve the system's depth accuracy, we placed a panda toy 8 m away from the transmitter and detected using focused illumination. The receiving FoV angle was 250 μrad. The first row of Figure 8 shows the intensity map, the second row shows the depth map; The figure shows that as the scanning step size decreased, the burrs around the toy quickly decreased and the contours become smoother and more accurate. The third row shows the depth profile at the position of the dotted line in the second row, where the depth differences were $d_B - d_A = 1545.6\ \text{mm} - 1538.4\ \text{mm} = 7.2\ \text{mm}$, $d_D - d_C = 1540.8\ \text{mm} - 1536.0\ \text{mm} = 4.8\ \text{mm}$, and $d_F - d_E = 1545.6\ \text{mm} - 1536.0\ \text{mm} = 9.6\ \text{mm}$. The depth differences indicated that the jitter matched the system's time jitter and reached a sub-centimeter level. Although sub-pixel scanning could make the target contour clearer, no significant improvement was observed in depth estimation compared with pixel-by-pixel scanning.

To observe the improvement of subpixel scanning on imaging resolution more intuitively, we reconstructed the 3D contour of the panda. The results in Figure 9 show that sub-pixel scanning can make the target imaging clearer and more accurate.

As mentioned earlier, these results were obtained using simple calculations. If a more sophisticated propagation model is constructed, pixel-wise cross-correlation can be performed using spatial correlations

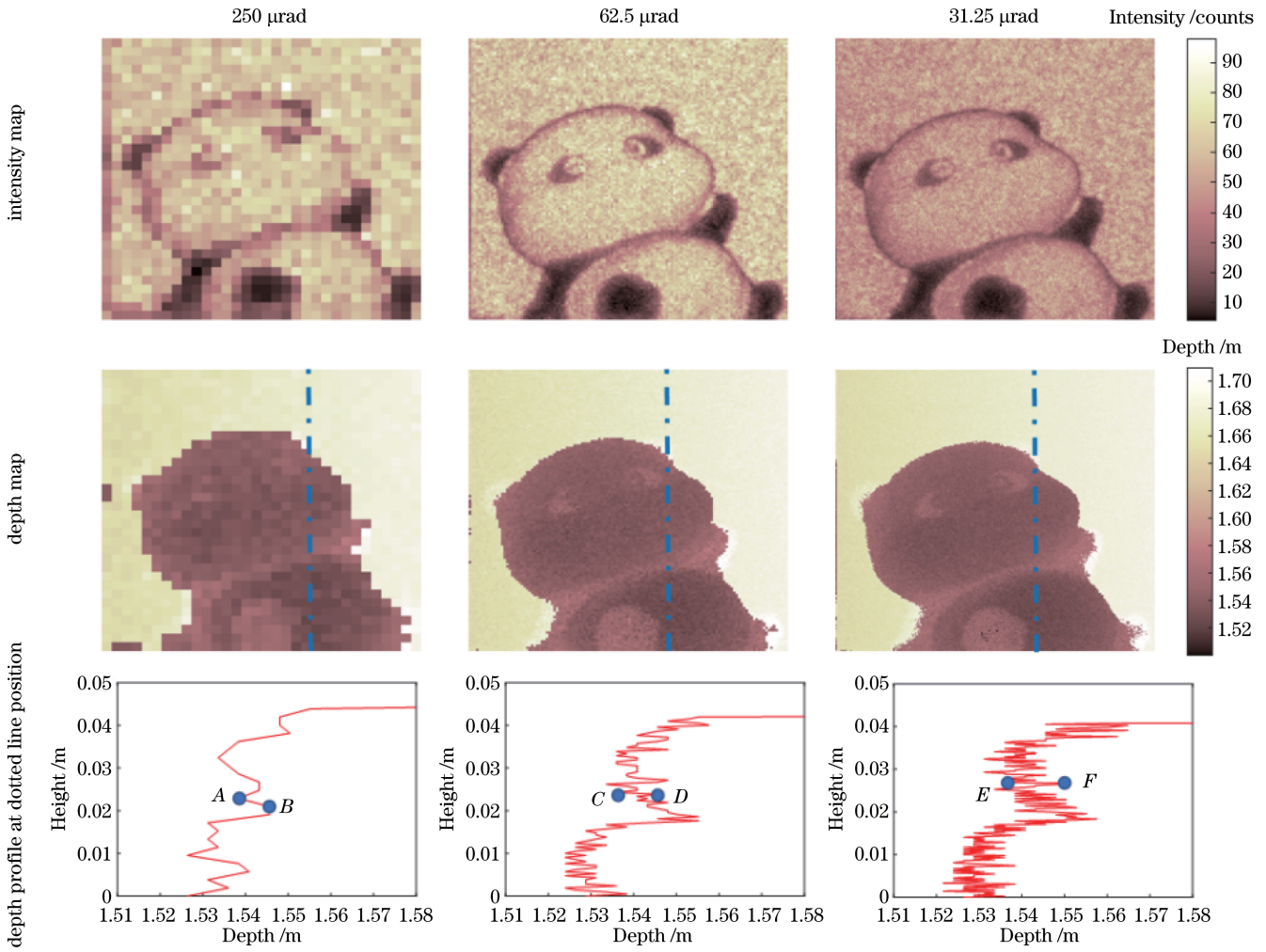

Fig. 8 Intensity and depth maps of panda doll illuminated by the focused beam at 8 m

between pixels, and high-resolution intensity and depth maps[30] can be combined to significantly improve the imaging results.

5 Conclusion

We demonstrated a sub-pixel scanning super-resolution technology using collimated and focused beams for illumination. At the same FoV, the imaging results of a transmission-resolution target showed that the imaging resolution can be effectively increased using small-beam illumination. The reconstructed images obtained through sub-pixel scanning were smoother and clearer than those obtained through pixel-by-pixel scanning. The lateral resolution increased from 5.0 mm per pixel collimation to 0.9 mm per pixel focus and exceeded the system angular resolution limit. In addition, the improvement effect of sub-pixel scanning on resolution was related to the spot size. Reducing the scanning step size infinitely is impractical owing to system scanning accuracy and scanning time limitations. Therefore, the sub-pixel scanning step size should be selected based on the measurement time, required resolution, and system limitations. The problem of long acquisition time can be solved by using large-step scanning initially to quickly search for the target, followed by sub-pixel scanning of the areas of interest. In future experiments, advanced algorithms can be employed, along with small-beam illumination and sub-pixel scanning, to further improve the imaging resolution of the system using certain abilities of Bessel beams to resist atmospheric turbulence[31], smoke[32], and the super-oscillatory beam′s sub-diffraction-limited central spot[33]. In conclusion, small-beam illumination and sub-pixel scanning technology have significant potential for improving the spatial resolution of long-distance lidar. Existing lidar systems rarely employ beam modulation techniques, particularly for scattering targets. Vector-focused illumination fields are expected to achieve higher resolutions in lidar and non-line-of-sight imaging[34].

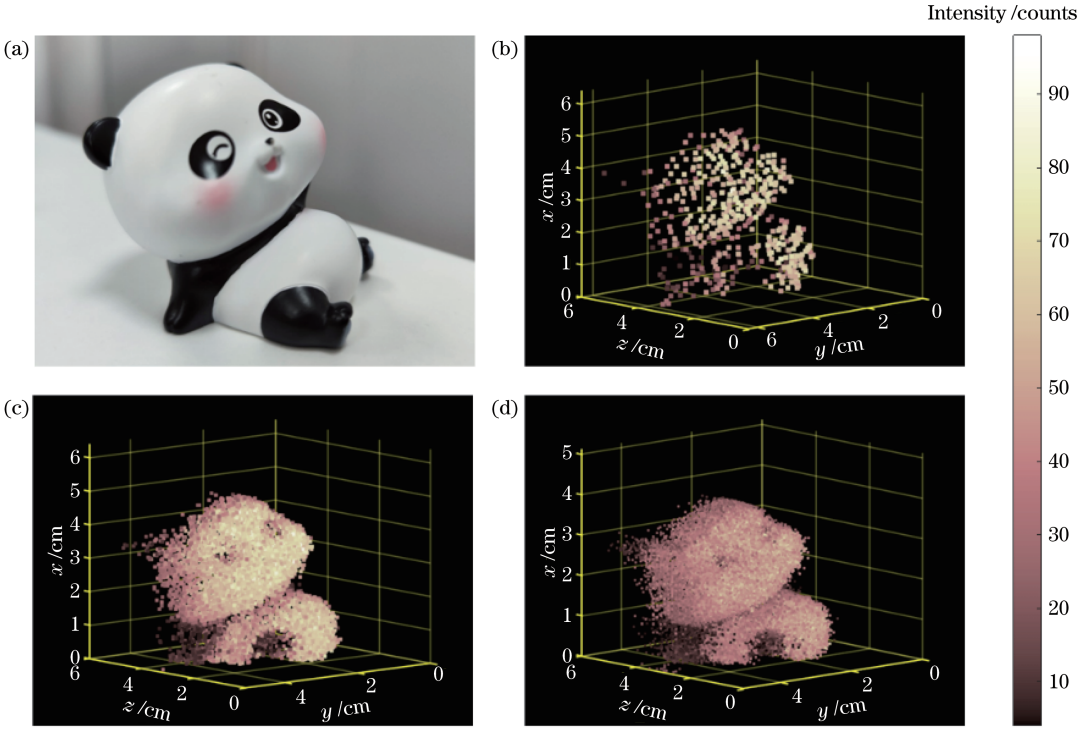

Fig. 9 3D reconstruction results of panda doll. (a) Picture of panda doll; (b) result of pixel-by-pixel scanning; (c) result of 1/4 sub-pixel scanning; (d) result of 1/8 sub-pixel scanning

References

[1] Swatantran A, Tang H, Barrett T, et al. Rapid, high-resolution forest structure and terrain mapping over large areas using single photon lidar[J]. Scientific Reports, 2016, 6: 28277.

[2] Degnan J J, Field C T. Moderate to high altitude, single photon sensitive, 3D imaging lidars[J]. Proceedings of SPIE, 2014, 9114: 91140H.

[3] Buyukdemircioglu M, Kocaman S. Reconstruction and efficient visualization of heterogeneous 3D city models[J]. Remote Sensing, 2020, 12(13): 2128.

[4] Bagheri H, Schmitt M, Zhu X X. Fusion of multi-sensor-derived heights and OSM-derived building footprints for urban 3D reconstruction[J]. ISPRS International Journal of Geo-Information, 2019, 8(4): 193.

[5] Yi S, Min S. A practical calibration method for stripe laser imaging system[J]. IEEE Transactions on Instrumentation and Measurement, 2021, 70: 5003307.

[6] Harmatys W, Gąska A, Gąska P, et al. Assessment of background illumination influence on accuracy of measurements performed on optical coordinate measuring machine equipped with video probe[J]. Sensors, 2021, 21(7): 2509.

[7] Du P F, Zhang F, Li Z P, et al. Single-photon detection approach for autonomous vehicles sensing[J]. IEEE Transactions on Vehicular Technology, 2020, 69(6): 6067-6078.

[8] Riemensberger J, Lukashchuk A, Karpov M, et al. Massively parallel coherent laser ranging using a soliton microcomb[J]. Nature, 2020, 581(7807): 164-170.

[9] Marino R M, Davis W R. Jigsaw: a foliage-penetrating 3D imaging laser radar system[J]. Lincoln Laboratory Journal, 2005, 15(1): 23-36.

[10] Huang G H, Shu R, Hou L B, et al. Design and performance of a fiber array coupled multi-channel photon counting, 3D imaging, airborne lidar system[J]. Proceedings of SPIE, 2014, 9080: 90800F.

[11] Kirmani A, Venkatraman D, Shin D, et al. First-photon imaging[J]. Science, 2014, 343(6166): 58-61.

[12] Pawlikowska A M, Halimi A, Lamb R A, et al. Single-photon three-dimensional imaging at up to 10 kilometers range[J]. Optics Express, 2017, 25(10): 11919-11931.

[13] Li Z P, Ye J T, Huang X, et al. Single-photon imaging over 200 km[J]. Optica, 2021, 8(3): 344-349.

[14] Li Z H, Wu E, Pang C K, et al. Multi-beam single-photon-counting three-dimensional imaging lidar[J]. Optics Express, 2017, 25(9): 10189-10195.

[15] McCarthy A, Collins R J, Krichel N J, et al. Long-range time-of-flight scanning sensor based on high-speed time-correlated single-photon counting[J]. Applied Optics, 2009, 48(32): 6241-6251.

[16] Li Z P, Huang X, Cao Y, et al. Single-photon computational 3D imaging at 45 km[J]. Photonics Research, 2020, 8(9): 1532-1540.

[17] Gao L, Shao L, Higgins C D, et al. Noninvasive imaging beyond the diffraction limit of 3D dynamics in thickly fluorescent specimens[J]. Cell, 2012, 151(6): 1370-1385.

[18] Singh B K, Nagar H, Roichman Y, et al. Particle manipulation beyond the diffraction limit using structured super-oscillating light beams[J]. Light: Science & Applications, 2017, 6(9): e17050.

[19] Perinchery S M, Haridas A, Shinde A, et al. Breaking diffraction limit of far-field imaging via structured illumination Bessel beam microscope (SIBM)[J]. Optics Express, 2019, 27(5): 6068-6082.

[20] Li Z P, Huang X, Jiang P Y, et al. Super-resolution single-photon imaging at 8.2 kilometers[J]. Optics Express, 2020, 28(3): 4076-4087.

[21] Xue R K, Kang Y, Zhang T Y, et al. Sub-pixel scanning high-resolution panoramic 3D imaging based on a SPAD array[J]. IEEE Photonics Journal, 2021, 13(4): 3900106.

[22] Guo J J, Fei X Y, Ge P, et al. High-resolution three-dimensional imaging based on all-fiber photon-counting Lidar system[J]. Infrared and Laser Engineering, 2021, 50(7):

20210162.

[23] Park S C, Park M K, Kang M G. Super-resolution image reconstruction: a technical overview[J]. IEEE Signal Processing Magazine, 2003, 20(3): 21-36.

[24] Zheng G A, Lee S A, Yang S, et al. Sub-pixel resolving optofluidic microscope for on-chip cell imaging[J]. Lab on a Chip, 2010, 10(22): 3125-3129.

[25] Ling F, Du Y, Xiao F, et al. Super-resolution land-cover mapping using multiple sub-pixel shifted remotely sensed images [J]. International Journal of Remote Sensing, 2010, 31(19): 5023-5040.

[26] Lin W Y, Panusopone K, Baylon D M, et al. A fast sub-pixel motion estimation algorithm for H.264/AVC video coding[J]. IEEE Transactions on Circuits and Systems for Video Technology, 2011, 21(2): 237-242.

[27] Murn L, Smeaton A F, Mrak M. Interpreting super-resolution CNNs for sub-pixel motion compensation in video coding[C]// Proceedings of the 29th ACM International Conference on Multimedia, October 20-24, 2021, Virtual Event, China. New York: ACM Press, 2021: 3803-3806.

[28] Yin W Y, He W J, Gu G H, et al. Approach for LIDAR signals with multiple returns[J]. Applied Optics, 2014, 53(30): 6963-6969.

[29] Shin D, Xu F H, Wong F N C, et al. Computational multi-depth single-photon imaging[J]. Optics Express, 2016, 24(3): 1873-1888.

[30] Gyongy I, Hutchings S W, Halimi A, et al. High-speed 3D sensing via hybrid-mode imaging and guided upsampling[J]. Optica, 2020, 7(10): 1253-1260.

[31] Meyers R E, Deacon K S, Tunick A D, et al. Virtual ghost imaging through turbulence and obscurants using Bessel beam illumination[J]. Applied Physics Letters, 2012, 100(6): 061126.

[32] Shi H T, Shen G Y, Qi H Y, et al. Noise-tolerant Bessel-beam single-photon imaging in fog[J]. Optics Express, 2022, 30(7): 12061-12068.

[33] Zheludev N I, Yuan G H. Optical superoscillation technologies beyond the diffraction limit[J]. Nature Reviews Physics, 2022, 4 (1): 16-32.

[34] Cao R Z, de Goumoens F, Blochet B, et al. High-resolution non-line-of-sight imaging employing active focusing[J]. Nature Photonics, 2022, 16(6): 462-468.